united nations
educational, scientific
and cultural
organization

international atomic
energy agency

the
abdus salam
international centre for theoretical physics

SMR: 1133/17

WINTER COLLEGE ON
SPECTROSCOPY AND APPLICATIONS

(8 - 26 February 1999)

"Lectures on Molecular Spectroscopy"

presented by:

Wolfgang DEMTRÖDER
Universität Kaiserslautern
Fachbereich Physik
Erwin-Schrodinger Strasse
67663 Kaiserslautern
Germany

Lectures on Molecular Spectroscopy

W. Demtröder, Fachbereich Physik,
Universität Kaiserslautern

1. Introduction:

There are three main experimental techniques, which can give information on molecular structure and dynamics and on the interaction between different atoms and molecules:

These are:

a) Spectroscopy
b) Scattering experiments
c) Macroscopic measurements, such as the study of transport phenomena (viscosity, diffusion, heat conduction) and of macroscopic properties, such as the relation between pressure, volume and temperature of a medium.

From all of these methods, spectroscopy certainly gives the most detailed and most accurate answers.

Most of our knowledge about the structure of atoms and molecules is based on spectroscopic investigations. Thus spectroscopy has made an outstanding contribution to the present state of atomic and molecular physics, to chemistry and molecular biology. Information on molecular structure and on the interaction of molecules with their surroundings may be derived in various ways from the absorption or emission spectra generated when electromagnetic radiation interacts with matter.

Wavelength measurements of spectral lines allow the determination of energy levels of the atomic or molecular system. The *line intensity* is proportional to the transition probability which measures how strongly the two levels of a molecular transition are coupled. Since the transition probability depends on the wave functions of both levels, intensity measurements are useful to verify the spatial charge distribution of excited electrons, which can only be roughly calculated from approximate solutions of the Schrödinger equation. The *natural linewidth* of a spectral line may be resolved by special techniques, allowing mean lifetimes of excited molecular states to be

determined. Measurements of the *Doppler width* yield the velocity distribution of the emitting or absorbing molecules and with it the temperature of the sample. From *pressure broadening* and *pressure shifts* of spectral lines, information about collision processes and interatomic potentials can be extracted. *Zeemann* and *Stark splittings* by external magnetic or electric fields are important means of measuring magnetic or electric moments and elucidating the coupling of the different angular momenta in atoms or molecules, even with complex electron configurations. The *hyperfine structure* of spectral lines yields information about the interaction between the nuclei and the electron cloud and allows nuclear magnetic dipole moments or electric quadrupole moments to be determined. Time resolved measurements allow the spectroscopist to follow up dynamical processes in ground state and excited state molecules, to investigate collision processes and various energy transfer mechanisms.

These examples represent only a small selection of the many possible ways by which spectroscopy provides tools to explore the microworld of atoms and molecules. However, the amount of information which can be extracted from a spectrum depends essentially on the attainable spectral or time resolution and on the detection sensitivity that can be achieved.

The application of new technologies to optical instrumentation (for instance, the production of larger and better ruled gratings in spectrographs, the use of highly reflecting dielectric coatings in interferometers, and the development of optical multichannel analysers and image intensifiers) has certainly significantly extended the sensitivity limits. Considerable progress was furthermore achieved through the introduction of new spectroscopic techniques such as Fourier spectroscopy, optical pumping, level-crossing techniques, and various kinds of double-resonance methods and molecular beam spectroscopy.

Although these new techniques have proved to be very fruitful, the really stimulating impetus to the whole field of spectroscopy was given by the introduction of lasers. In many cases these new spectroscopic light sources may increase spectral resolution and sensitivity by several orders of magnitude. Combined with new spectroscopic techniques, lasers are able to surpass basic limitations of classical spectroscopy. Many experiments that could not be performed with incoherent light sources are now feasible or have already been successfully completed recently. These lectures discuss such new techniques of laser spectroscopy and explain the necessary instrumentation.

3. Advantages of Lasers in Spectroscopy

In order to illustrate the advantages of absorption spectroscopy with tunable lasers, at first we compare it with the conventional absorption spectroscopy which uses incoherent radiation sources. Figure 6.1 presents schematic diagrams for both methods.

In classical absorption spectroscopy, radiation sources with a *broad emission continuum* are preferred (e.g., high-pressure Hg arcs, Xe flash lamps, etc.). The radiation is collimated by the lens L_1 and passes through the absorption cell. Behind a dispersing instrument for wavelength selection (spectrometer or interferometer) the intensity $I_T(\lambda)$ of the transmitted light is measured as a function of the wavelength λ (Fig.6.1a). By comparison with the reference beam $I_R(\lambda)$ (which can be realized, for instance, by shifting the absorption cell alternatively out of the light beam) the absorption spectrum

$$I_A(\lambda) = a[I_0(\lambda) - I_T(\lambda)] = a[bI_R(\lambda) - I_T(\lambda)]$$

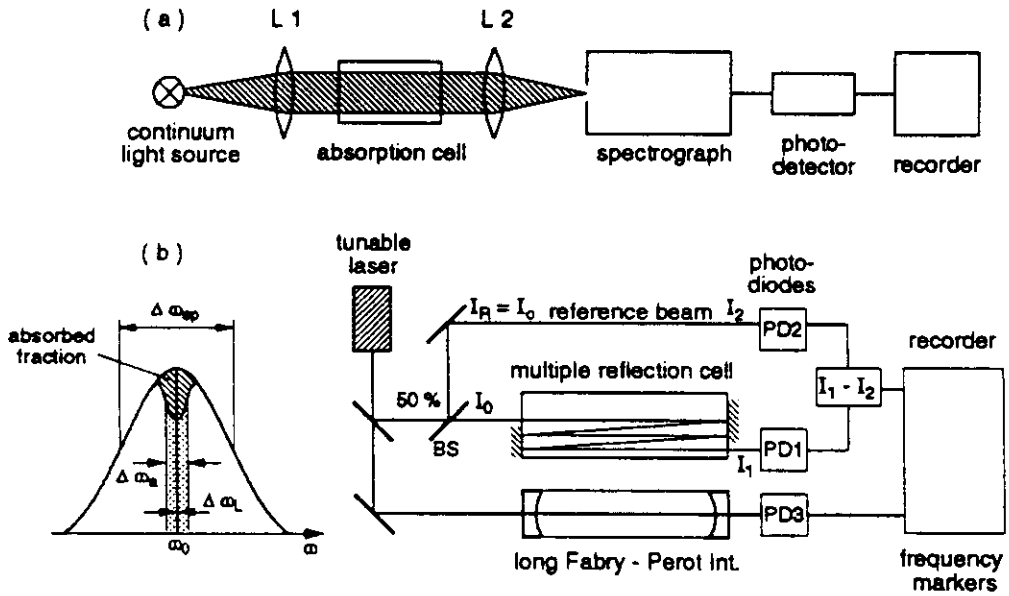

Fig.6.1. Comparison between absorption spectroscopy with a broadband incoherent source (a) and with a tunable single-mode laser (b)

can be obtained, where the constants a and b take into account wavelength-independent losses of I_R and I_T (e.g., reflections of the cell walls).

The *spectral resolution* is generally limited by the resolving power of the dispersing spectrometer. Only with large and expensive instruments (e. g., Fourier spectrometers) may the Doppler limit be reached [6.1].

The *detection sensitivity* of the experimental arrangement is defined by the minimum absorbed power which can still be detected. In most cases it is limited by the detector noise and by intensity fluctuations of the radiation source. Generally the limit of the detectable absorption is reached at relative absorptions $\Delta I/I \geq 10^{-4}$-10^{-5}. This limit can be pushed further down only in favorable cases by using special sources and lock-in detection or signal-averaging techniques.

Contrary to radiation sources with broad emission continua used in conventional spectroscopy, tunable lasers offer radiation sources in the spectral range from the UV to the IR with extremely narrow bandwidths and with spectral power densities which may exceed those of incoherent light sources by many orders of magnitude (Sects.5.7,8).

In several regards laser absorption spectroscopy corresponds to microwave spectroscopy where clystrons or carcinotrons instead of lasers represent tunable coherent radiation sources. Laser spectroscopy transfers many of the techniques and advantages of microwave spectroscopy to the infrared, visible, and ultraviolet spectral ranges.

The advantages of absorption spectroscopy with tunable lasers may be summarized as follows:

- No monochromator is needed since the absorption coefficient $\alpha(\omega)$ and its frequency dependence can be directly measured from the difference $\Delta I(\omega) = a[I_R(\omega) - I_T(\omega)]$ between the intensities of the reference beam with $I_R = I_2$ and transmitted beam $T_T = I_1$ (Fig.6.1b). The spectral resolution is higher than in conventional spectroscopy. With tunable single-mode lasers it is only limited by the linewdiths of the absorbing molecular transitions. Using Doppler-free techniques (Chaps.7-10), even sub-Doppler resolution can be achieved.

- Because of the high spectral power density of many lasers, the detector noise is generally negligible. Intensity fluctuations of the laser which limit the detection sensitivity, may essentially be suppressed by intensity stabilization (Sect.5.4). This furthermore increases the signal-to-noise ratio and therefore enhances the sensitivity.

- The detection sensitivity increases with increasing spectral resolution $\omega/\Delta\omega$ as long as $\Delta\omega$ is still larger than the linewidth $\delta\omega$ of the absorption line. This can be seen as follows.

The relative intensity attenuation per absorption path length x = 1 cm on the transition with center frequency ω_0 is for small absorption $\alpha x << 1$

$$\Delta I/I = \int_{\omega_0 - \frac{1}{2}\Delta\omega}^{\omega_0 + \frac{1}{2}\Delta\omega} \alpha(\omega)\, I(\omega)\, d\omega \Big/ \int_{\omega_0 - \frac{1}{2}\delta\omega}^{\omega_0 + \frac{1}{2}\delta\omega} I(\omega)\, d\omega \,. \qquad (6.1)$$

If $I(\omega)$ does not change much within the interval $\Delta\omega$ we can write

$$\int_{\omega_0-\frac{1}{2}\Delta\omega}^{\omega_0+\frac{1}{2}\Delta\omega} I(\omega)\,d\omega = \bar{I}\,\Delta\omega \quad \text{and} \quad \int\alpha(\omega)\,I(\omega)\,d\omega = \bar{I}\int\alpha(\omega)\,d\omega\,.$$

This yields

$$\frac{\Delta I}{I} = \frac{1}{\Delta\omega}\int_{\omega_0-\frac{1}{2}\delta\omega}^{\omega_0+\frac{1}{2}\delta\omega}\alpha(\omega)\,d\omega \simeq \bar{\alpha}\,\frac{\delta\omega}{\Delta\omega} \quad \text{for} \quad \Delta\omega > \delta\omega\,. \tag{6.2}$$

Example 6.1

The spectral resolution of a 1-m spectrograph is about 0.1 Å, which corresponds at $\lambda = 500$ nm to $\Delta\omega = 2\pi \cdot 12$ GHz. The Doppler width of gas molecules with M = 30 at T = 300 K is, according to (3.43) $\delta\omega \simeq 2\pi \cdot 1$ GHz. With a single-mode laser the value of $\delta\omega$ becomes smaller than $\Delta\omega$ and the observable signal $\Delta I/I$ becomes 12 times larger.

• Because of the good collimation of a laser beam, long absorption paths can be realized by multiple reflection back and forth through the multiple-path absorption cell. Disturbing reflections from cell walls or windows which may influence the measurements can essentially be avoided (for example, by using Brewster end windows). Such long absorption paths enable measurements of transitions even with small absorption coefficients. Furthermore pressure broadening can be reduced by using low gas pressure. This is especially important in the infrared region where the Doppler width is small and the pressure broadening may become the limiting factor for the spectral resolution (Sect.3.3).

Example 6.2

With an intensity stabilized light source and lock-in detection the minimum relative absorption which may be safely detected, is about $\Delta I/I \geq 10^{-6}$, which yields the minimum measurable absorption coefficient for an absorption pathlength L

$$\alpha \geq \frac{10^{-6}}{L}\,\frac{\Delta\omega}{\delta\omega} \quad [\mathrm{cm}^{-1}]\,,$$

For L = 10 cm and $\delta\omega = 10\Delta\omega$ we obtain $\alpha \geq 10^{-6}$ cm^{-1}. With single-mode lasers one may reach $\Delta\omega < \delta\omega$ and L = 10 m which yields a minimum detectable absorption coefficient of $\alpha \geq 10^{-9}$ cm^{-1}, i.e. an improvement of a factor of 1000 !

- If a small fraction of the laser output is sent through a long Fabry-Perot interferometer with a separation d of the mirrors, the photodetector PD3 receives intensity peaks each time the laser frequency ν_L is tuned to a transmission maximum at $\nu = \frac{1}{2}mc/d$ (Sects.4.2,4). These peaks serve as accurate wavelength markers which allow one to calibrate the separation of adjacent absorption lines (Fig.6.1). With d = 1 m the frequency separation $\Delta\nu_p$ between successive transmission peaks is $\Delta\nu_p = c/2d = 150$ MHz, corresponding to a wavelength separation of 10^{-4} nm at $\lambda = 550$ nm. With a semiconfocal FPI the free spectral range is c/8d, which gives $\Delta\nu_p = 75$ MHz for d = 0.5 m.

- The laser frequency may be stabilized onto the center of an absorption line. With the methods discussed in Sect.4.4 it is possible to measure the wavelength λ_L of the laser with an absolute accuracy of 10^{-8} or better. This allows determination of the molecular absorption lines with the same accuracy.

- It is possible to tune the laser wavelength very rapidly over a spectral region where molecular absorption lines have to be detected. With electro-optical components, for instance, pulsed dye lasers can be tuned over several wave numbers within a microsecond. This opens new perspectives for spectroscopic investigations of short-lived intermediate radicals in chemical reactions. The capabilities of classical flash photolysis may be considerable extended using such rapidly tunable laser sources.

- An important advantage of absorption spectroscopy with tunable single-mode lasers stems from their capabilites to measure line profiles of absorbing molecular transitions with high accuracy. In case of pressure broadening the determination of line profiles allows one to derive information about the interaction potential of the collision partners (Sects.3.3 and 13.1). In plasma physics this technique is widely used to determine electron and ion densities and temperatures.

- In fluorescence spectroscopy and optical pumping experiments, the high intensity of lasers allows an appreciable population in selectively excited states to be achieved which may be comparable to that of the absorbing ground states. The small laser linewidth favors the selectivity of optical excitation and results in favorable cases in the exclusive population of single molecular levels. These advantageous conditions allow one to perform absorption and fluorescence spectroscopy of *excited* states and to transform spectroscopic methods, such as microwave or RF spectroscopy, which has up to now been restricted to electronic ground states, also to excited states.

This brief overview of some advantages of lasers in spectroscopy will be outlined in more detail in the following chapters and several examples will illustrate their relevance.

4. High-Sensitivity Methods of Absorption Spectroscopy

The general method for measuring absorption spectra is based on the determination of the absorption coefficient $\alpha(\omega)$ from the spectral intensity

$$I_T(\omega) = I_0 \exp[-\alpha(\omega)x] \tag{6.3}$$

which is transmitted through an absorbing path length x. For small absorption $\alpha x << 1$ we can use the approximation $\exp(-\alpha x) \simeq 1-\alpha x$, and (6.3) can be reduced to

$$I_T(\omega) \simeq I_0[1 - \alpha(\omega)x] . \tag{6.4}$$

With the reference intensity $I_R = I_0$, as produced, for example, by a 50% beam splitter with the reflectivity R = 0.5 (Fig.6.1b), one can measure the absorption coefficient

$$\alpha(\omega) = \frac{I_R - I_T(\omega)}{I_R x} \tag{6.5}$$

from the difference $\Delta I = I_R - I_T(\omega)$.

The absorption coefficient $\alpha_{ik}(\omega)$ of the transition $|i\rangle \rightarrow |k\rangle$ with an absorption cross section σ_{ik} is determined by the density N_i of absorbing molecules:

$$\alpha_{ik}(\omega) = [N_i - (g_i/g_k)N_k]\sigma_{ik}(\omega) = \Delta N \sigma_{ik}(\omega) . \tag{6.6}$$

If the population N_k is small compared to N_i, we obtain from (6.6) for the minimum detectable density N_i over the absorption path length x = L:

$$\boxed{N_i \geq \frac{\Delta I}{I_0 L \sigma_{ik}} .} \tag{6.7}$$

The minimum, still detectable concentration N_i of absorbing molecules is determined by the absorption path length L, the absorption cross section σ_{ik}, and the minimum detectable, relative intensity change $\Delta I/I_0$ caused by absorption.

In order to reach a high detection sensitivity for absorbing molecules, $L\sigma_{ik}$ should be large and the minimum detectable value of $\Delta I/I$ as small as possible.

In the case of very small values of αx, this method in which the attenuation of the transmitted light is measured, cannot be very accurate since it has to determine a small difference $I_0 - I_T$ of two large quantities I_0 and I_T. Small fluctuations of I_0 or of the splitting ratio of the beam splitter BS in Fig.6.1b can already severely influence the measurement. Therefore, other techniques have been developed leading to an increase of sensitivity and accuracy of absorption measurements by several orders of magnitude compared to direct absorption measurements. These sensitive detection methods represent remarkable progress, since their sensitivity limits have been pushed from relative absorptions $\Delta\alpha/\alpha \simeq 10^{-5}$ down to about $\Delta\alpha/\alpha \geq 10^{-17}$. We now discuss these different methods in more detail.

4..1 Frequency Modulation

The first scheme to be treated is based on a frequency modulation of the monochromatic incident wave. It has not been designed specifically for laser spectroscopy but was taken from microwave spectroscopy where it is a standard method. The laser frequency ω_L is modulated at the modulation frequency f, which tunes ω_L periodically from ω_L to $\omega_L + \Delta\omega_L$. When the laser is tuned through the absorption spectrum, the difference $I_T(\omega_L) - I_T(\omega_L + \Delta\omega_L)$ is detected with a lock-in amplifier (phase-sensitive detector) tuned to the modulation frequency (Fig.6.2). If the modulation sweep $\Delta\omega_L$ is sufficiently small, the first term of the Taylor expansion

$$I_T(\omega_L + \Delta\omega_L) - I_T(\omega_L) = \frac{dI_T}{d\omega}\Delta\omega_L + \frac{1}{2!}\frac{d^2 I_T}{d\omega^2}\Delta\omega_L^2 + \ldots \qquad (6.8)$$

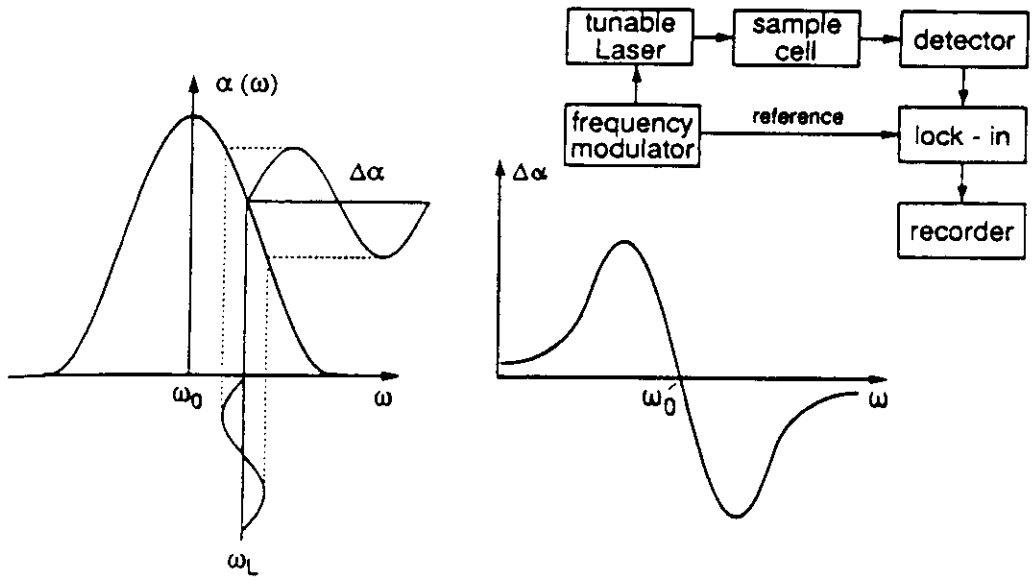

Fig.6.2. Absorption spectroscopy with a frequency modulated single-mode laser

is dominant. This term is proportional to the first derivative of the absorption spectrum, as can be seen from (6.5): When I_R is independent of ω we obtain for the absorption length L

$$\frac{d\alpha(\omega)}{d\omega} = -\frac{1}{I_R L}\frac{dI_T}{d\omega}. \qquad (6.9)$$

If the laser frequency

$$\omega_L(t) = \omega_0 + a\sin\Omega t$$

is sinusoidally modulated at a modulation frequency Ω the Taylor expansion yields

$$I_T(\omega_L) = I_T(\omega_0) + \sum_n \frac{a^n}{n!}\sin^n\Omega t \left(\frac{d^n I_T}{d\omega^n}\right)_{\omega_0} . \qquad (6.10)$$

For $\alpha L << 1$ we obtain from (6.4)

$$\left(\frac{d^n I_T}{d\omega^n}\right)_{\omega_0} = - I_0 x \left(\frac{d^n \alpha(\omega)}{d\omega^n}\right)_{\omega_0} .$$

The terms $\sin^n\Omega t$ can be converted into linear functions of $\sin(n\Omega t)$ and $\cos(n\Omega t)$ using known trigonometric formula.

Inserting these relations into (6.10) one finds after rearrangement of the terms the expression

$$\begin{aligned}\frac{I_T(\omega_L) - I_T(\omega_0)}{I_0} = - aL\Bigg\{&\left[\frac{a}{4}\left(\frac{d^2\alpha}{d\omega^2}\right)_{\omega_0} + \frac{a^3}{64}\left(\frac{d^4\alpha}{d\omega^4}\right)_{\omega_0} + \ldots\right] \\ &+ \left[\left(\frac{d\alpha}{d\omega}\right)_{\omega_0} + \frac{a^2}{8}\left(\frac{d^3\alpha}{d\omega^3}\right)_{\omega_0} + \ldots\right]\sin(\Omega t) \\ &+ \left[-\frac{a}{4}\left(\frac{d^2\alpha}{d\omega^2}\right)_{\omega_0} + \frac{a^3}{48}\left(\frac{d^4\alpha}{d\omega^4}\right)_{\omega_0} + \ldots\right]\cos(2\Omega t) \\ &+ \left[-\frac{a^2}{24}\left(\frac{d^3\alpha}{d\omega^3}\right)_{\omega_0} + \frac{a^4}{384}\left(\frac{d^5\alpha}{d\omega^5}\right)_{\omega_0} + \ldots\right]\sin(3\Omega t) + \ldots\Bigg\} .\end{aligned}$$

For a sufficiently small modulation amplitude ($a/\omega_0 << 1$) the first terms in each bracket are dominant and we obtain for the signal $S(n\Omega)$ behind a lock-in amplifier, tuned to the frequency $n\Omega$ (Fig.6.3):

$$S(n\Omega) = \left(\frac{I_T(\omega_L) - I_T(\omega_0)}{I_0}\right)_{n\Omega} = aL\begin{cases} b_n \sin(n\Omega t) & \text{for } n = 2m+1 \\ c_n \cos(n\Omega t) & \text{for } n = 2m . \end{cases}$$

In particular, the signals for the first three derivatives of the absorption coefficient $\alpha(\omega)$, shown in Fig.6.3, are

$$S(\Omega) = - aL \frac{d\alpha}{d\omega} \sin(\Omega t)$$

$$S(2\Omega) = + \frac{a^2 L}{4} \frac{d^2\alpha}{d\omega^2} \cos(2\Omega t) \qquad (6.11)$$

$$S(3\Omega) = + \frac{a^3 L}{24} \frac{d^3\alpha}{d\omega^3} \sin(3\Omega t) \, .$$

The advantage of this "derivative spectroscopy" [6.2] with a frequency modulation of the laser is the possibility for phase-sensitive detection, which restricts the frequency response of the detection system to a narrow frequency interval centered at the modulation frequency Ω. Frequency-independent background absorption from cell windows and background noise due to fluctuations of the laser intensity or of the density of absorbing molecules are essentially reduced. Regarding the signal-to-noise ratio and achievable sensitivity, the *frequency* modulation technique is superior to an *intensity* modulation of the incident radiation. The frequency of a single-mode laser can readily be modulated when an AC voltage is applied to the piezo onto which a resonator mirror is mounted (Sect.5.5).

The technical noise which represents the major limitation decreases with increasing frequency. It is therefore advantageous to choose the modulation frequency as high as possible. For diode lasers this can be achieved by modulation of the diode current. For other lasers, often electro-optical modulators outside the laser resonator are used as phase modulators resulting in a frequency modulation of the transmitted laser beam [6.3].

If the modulation frequency Ω is chosen sufficiently high (Ω > 1000 MHz) the technical noise may drop below the quantum-noise limit set by the statistical fluctuations of detected photons. In this case the detection limit is mainly due to the quantum limit [6.4].

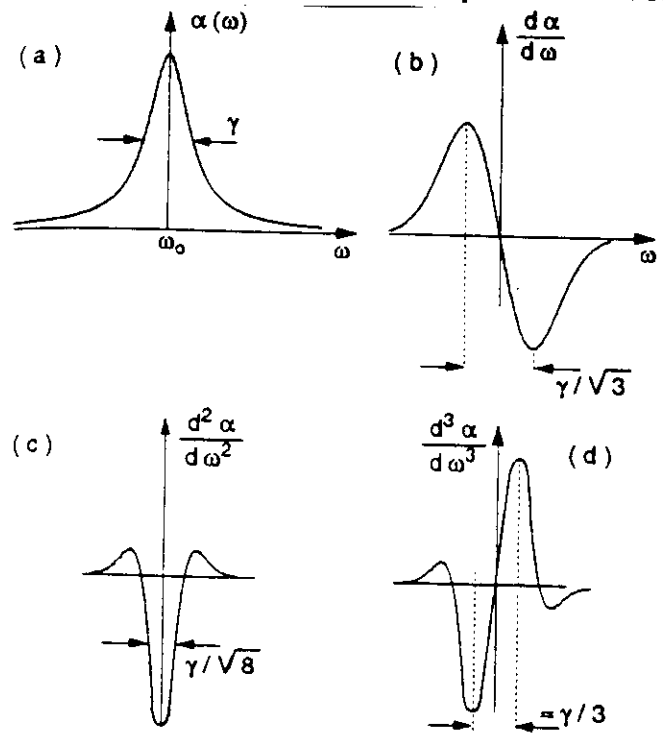

Fig.6.3. Lorentzian line profile $\alpha(\omega)$ of halfwidth γ (FWHM) (a) with first (b) second (c) and third (d) derivatives

4.2 Photoacoustic Spectroscopy

This sensitive technique for measuring small absorptions is mainly applied when minute concentrations of molecular species have to be detected in the presence of other components at higher pressure. An example is the detection of spurious pollutant gases in the atmosphere. Its basic principle may be summarized as follows:

The laser beam is sent through the absorber cell (Fig.6.13). If the laser is tuned to the absorbing molecular transition $E_i \rightarrow E_k$, part of the molecules in the lower level E_i will be excited into the upper level E_k. By collisions with other atoms or molecules in the cell these excited molecules may tansfer their excitation energy $(E_k - E_i)$ completely or partly into translational, rotational, or vibrational energy of the collision partners. At thermal equilibrium, this energy is randomly distributed onto all degrees of freedom, causing an increase of thermal energy and with it a rise of temperature and pressure at a constant density in the cell.

When the laser beam is chopped at frequencies below 20 kHz, periodical pressure variations appear in the absorption cell which can be detected with a sensitive microphone placed inside the cell. The output signal S [Volt] of the microphone is proportional to the pressure change Δp induced by the absorbed radiation power ΔW. If saturation can be neglected, the absorbed energy per cycle

$$\Delta W = N_i \sigma_{ik} \Delta x (1 - \eta_K) P_L \Delta t \tag{6.23}$$

is proportional to the density N_i [cm^{-3}] of the absorbing molecules in level |i), the absorption cross section σ_{ik} [cm^2], the absorption pathlength Δx, the cycle period Δt, and the incident laser power P_L. The signal decreases with increasing quantum efficiency η_k (which gives the ratio of emitted fluorescence energy to absorbed laser energy) unless the fluorescence is absorbed inside the cell and contributes to the temperature rise.

Since the absorbed energy ΔW is transferred into kinetic or internal energy of all N molecules per cm^3 in the photoacoustic cell with the volume V, the temperature rise ΔT is obtained from

$$\Delta W = \tfrac{1}{2} f V N k \Delta T \tag{6.24}$$

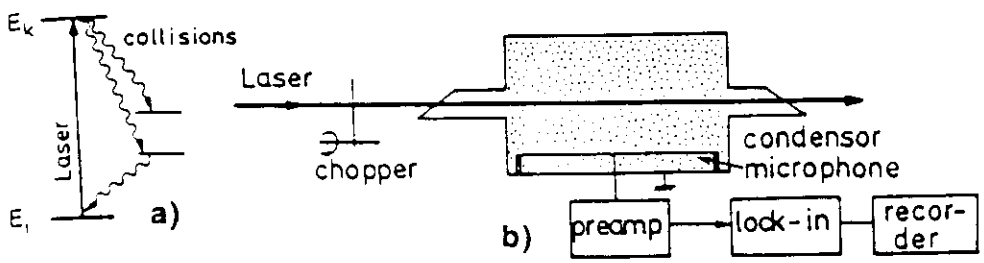

Fig.6.13. Photoacoustic spectroscopy (a) level scheme (b) schematic experimental arrangement

where f is the number of degrees of freedom, that are accessible for each of the N molecules at the temperature T [K]. If the chopping frequency of the laser is sufficiently high, the heat transfer to the walls of the cell during the pressure risetime can be neglected. From the equation of state $pV = NVkT$ we finally obtain

$$\Delta p = Nk\Delta T = \frac{2\Delta W}{fV} . \tag{6.25}$$

The output signal S from the microphone is then

$$S = \Delta p S_m = \frac{2N_i \sigma_{ik}}{fV} \Delta x (1 - \eta_k) P_L \Delta t S_m \tag{6.26}$$

where the sensitivity S_m [Volt/Pascal] of the microphone not only depends on the characteristics of the microphone but also on the geometry of the photoacoustic cell.

With infrared lasers the molecules are generally excited into higher vibrational levels of the electronic ground state. Assuming cross sections of $10^{-18} - 10^{-19}$ cm^2 for the collisional deactivation of the vibrationally excited molecules, the equipartition of energy takes only about 10^{-5} s at pressures around 1 Torr. Since the spontaneous lifetimes of these excited vibrational levels are typically around $10^{-2} - 10^{-5}$ s, it follows that at pressures above 1 Torr the excitation energy, absorbed from the laser beam, will be almost completely transferred into thermal energy, which implies that $\eta_k \sim 0$.

The idea of the spectraphone is very old and was already demonstrated by Bell and Tyndal [6.31] in 1881. However, the impressive detection sensitivity obtained nowadays could only be achieved with the development of lasers, sensitive capacitance microphones, low-noise amplifiers, and lock-in techniques. Concentrations down to the ppb range (parts per billion = 10^{-9}) at total pressures of 1 Torr to several atmospheres are readily detectable with a modern spectraphone (Fig.6.14).

Modern condensor microphones with a low-noise FET preamplifier and phase-sensitive detection achieve signals of larger than 1 V/Torr ($\hat{=}$7 mV/Pascal) with a background noise of $3 \cdot 10^{-8}$ V at integration times of

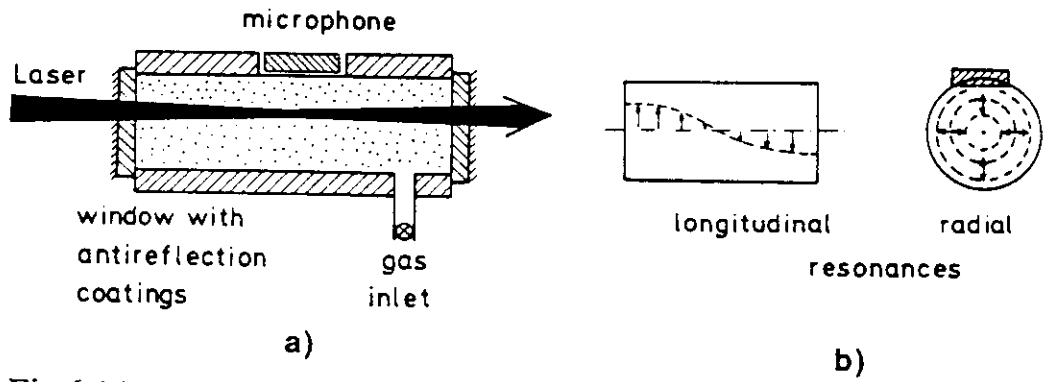

Fig.6.14. (a) Spectraphone with capacitance microphone (b) longitudinal and radial acoustic resonance modes

1 s. This sensitivity allows detection of pressure amplitudes below 10^{-7} Torr, and is, in general, not limited by the electronic noise but by another disturbing effect: Laser light reflected from the cell windows or scattered by aerosols in the cell may partly be absorbed by the walls and contributes to a temperature increase. The resulting pressure rise is, of course, modulated at the chopping frequency and is therefore detected as background signal. There are several ways to reduce this phenomenon. Antireflection coatings of the cell windows or, in case of linearly polarized laser light, the use of Brewster windows minimize the reflections. An elegant solution chooses the chopping frequency to coincide with an acoustic resonance of the cell. This results in a resonant amplification of the pressure amplitude which may be as large as 1000-fold. This experimental trick has the additional advantage that those acoustic resonances can be selected, which couple most efficiently to the beam profile but are less effectively excited by heat conduction from the walls. The background signal caused by wall absorption can thus be reduced and the true signal is enhanced. Figure 6.14b shows longitudinal and radial acoustic resonances in a cylindrical cell.

Example 6.7

With $N_i = 2.5 \cdot 10^{11}$ cm^{-3} ($\hat{=}$ 10^{-8} bar), $\sigma_{ik} = 10^{-16}$ cm^2, $\Delta x = 10$ cm, $V = 50$ cm^3, $\eta_k = 0$, $f = 6$ we obtain the pressure change $\Delta p = 1.5$ Pascal ($\hat{=}$0.01 Torr) for the incident laser power $P_L = 100$ mW. With a microphone sensitivity of $S_m = 10^{-2}$ V/Pascal the output signal becomes $S = 15$ mV.

The sensitivity can be further enhanced by frequency modulation of the laser (Sect.6.2.1) and by intracavity absorption techniques. With the spectraphone inside the laser cavity the photoacoustic signal due to nonsaturating transitions is increased by a factor q as a result of a q-fold increase of the laser intensity inside the resonator (Sect.6.2.2).

According to (6.26) the optoacoustic signal decreases with increasing quantum efficiency because the fluorescence carries energy away without heating the gas, as long as the fluorescence light is not absorbed within the cell. Since the quantum efficiency is determined by the ratio of spontaneous to collision-induced deactivation of the excited level, it decreases with increasing spontaneous lifetime and gas pressure. Therefore, the optoacoustic method is particularly favorable to monitor vibrational spectra of molecules in the infrared region (because of the long lifetimes of excited vibrational levels) and to detect small concentrations of molecules in the presence of other gases at higher pressures (because of the large collisional deactivation rate). It is even possible to use this technique for measuring *rotational* spectra in the microwave region and also electronic molecular spectra in the visible or ultraviolet range where electronic states with short spontaneous lifetimes are excited. However, the sensitivity in these spectral regions is not quite as high and there are other methods which are superior.

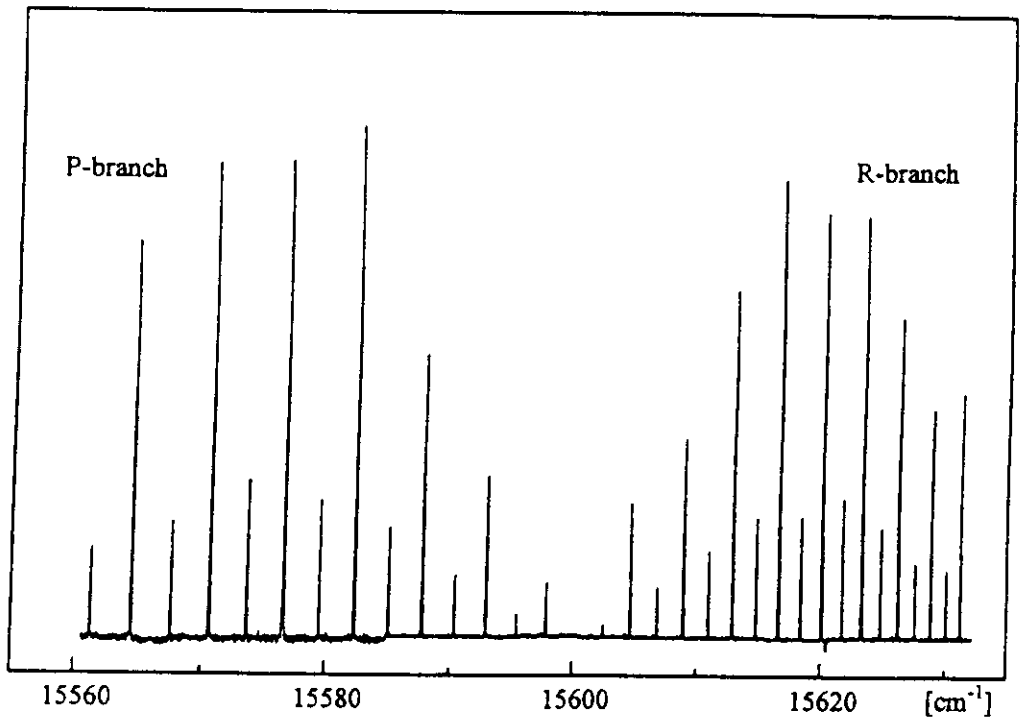

Fig.6.15. Optoacoustic overtone absorption spectrum of acethylene around $\tilde{\nu}$ = 15600 cm^{-1} corresponding to the excitation of a local mode by 5 quanta vibrations [6.45]

d) The application of photoacoustic detection to the visible region has been reported by *Stella* et al. [6.47]. They placed the spectraphone inside the cavity of a CW dye laser and scanned the laser across the absorption bands of the CH_4 and NH_3 molecules. The high-quality spectra with resolving power of over $2 \cdot 10^5$ proved to be adequate to resolve single rotational features of the very weak vibrational overtone transitions in these molecules. The experimental results prove to be very useful for the investigation of the planetary atmospheres where such weak overtone transitions are induced by the sun light.

e) An interesting application of photoacoustic detection lies in the measurement of dissociation energies of molecules [6.48]. When the laser wavelength is tuned across the dissociation limit, the photoacoustic signal drops drastically because beyond this limit the absorbed laser energy is used for dissociation (which means that it is converted into potential energy and cannot be tansferred into kinetic energy as in the case of excited-state deactivation. Only the kinetic energy causes a pressure increase).

f) With a special design of the spectraphone, employing a coated quartz membrane for the condensor microphone, even corrosive gases can be measured [6.49]. This extends the applications of optoacoustic spectroscopy to aggressive pollutant gases such as NO_2 or SO_2 which are important constituents of air pollution.

The photoacoustic spectroscopy can be also applied to liquids and solids [6.50]. An interesting application is the determination of species absorbed on surfaces. Optoacoustic spectroscopy allows a time-resolved analysis of adsorption- and desorption processes of atoms or molecules at liquid or solid surfaces, and their dependence on the surface characteristics and on the temperature [6.51].

4.3 Direct Determination of Absorbed Photons

In the methods discussed in the preceding sections the attenuation of the transmitted light (or of the laser power in intracavity spectroscopy) is monitored to determine the absorption coefficient $\alpha(\omega)$ or the number density of absorbing species. For small absorptions this means the measurement of a small difference of two large quantities which limits, of course, the signal-to-noise ratio.

Several different techniques have been developed, where the absorbed radiation power, i.e. the number of absorbed photons can be directly monitored. These techniques belong to the most sensitive detection methods in spectroscopy, and it is worthwhile to know about them.

4.3.1 Fluorescence Excitation Spectroscopy

In the visible and ultraviolet regions a very high sensitivity can be achieved, if the absorption of laser photons is monitored through the laser-induced fluorescence (Fig.6.10). When the laser wavelength λ_L is tuned to an absorbing molecular transition $E_i \rightarrow E_k$, the number of photons absorbed per second along the path length Δx is

$$n_a = N_i n_L \sigma_{ik} \Delta x \tag{6.20}$$

where n_L is the number of incident laser photons per second, σ_{ik} the absorption cross section per molecule, and N_i the density of molecules in the absorbing state $|i\rangle$.

The number of fluorescence photons emitted per second from the excited level E_k is

$$n_{fl} = N_k A_k = n_a \eta_k \ , \tag{6.21}$$

where $A_k = \sum_m A_{km}$ stands for the total spontaneous-transition probability (Sect.2.7) to all levels with $E_m < E_k$. The quantum efficiency of the excited state, $\eta_k = A_k/(A_k+R_k)$, gives the ratio of the spontaneous transition rate to the total deactivation rate which may also include the radiationless transition rate R_k (e.g., collision-induced transitions). For $\eta_k = 1$ the number n_{Fl} of fluorescence photons emitted per second equals the number n_a of photons absorbed per second under stationary conditions.

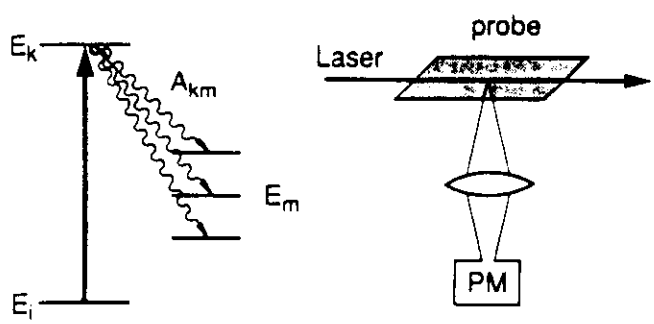

Fig.6.10. Level scheme and experimental arrangement for fluorescence excitation spectroscopy

Unfortunately only the fraction δ of the fluorescence photons emitted into all directions, can be collected on the photomultiplier cathode where again only the fraction $\eta_{ph} = n_{pe}/n_{ph}$ of these photons produces on the average n_{pe} photoelectrons. The quantity η_{ph} is called the *quantum efficiency of the photocathode* (Sect.4.5.2). The number n_{pe} of photoelectrons counted per second is then

$$n_{pe} = n_a \eta_k \eta_{ph} \delta = (N_i \sigma_{ik} n_L \Delta x) \eta_k \eta_{ph} \delta \, . \qquad (6.22)$$

Example 6.5

Modern photomultipliers reach quantum efficiencies of $\eta_{ph} = 0.2$. With carefully designed optics it is possible to achieve a collection factor $\delta = 0.1$. Using photon counting techniques and cooled multipliers (dark pulse rate $\leq$10 counts/s), counting rates of $n_{pe} = 100$ counts/s are already sufficient to obtain a signal-to-noise ratio S/R ~ 8 at integration times of 1s.

Inserting this figure for n_{PE} into (6.22) illustrates that with $\eta_k = 1$ absorption rates of $n_a = 5 \cdot 10^3$/s can already be measured quantitatively. Assuming a laser power of 1 W at the wavelength $\lambda = 500$ nm which corresponds to a photon flux of $n_L = 3 \cdot 10^{18}$/s, this implies *that it is possible to detect a relative absorption of* $\Delta I/I \leq 10^{-14}$. When placing the absorbing probe inside the cavity where the laser power is q times larger (q ~ 10 to 100, Sect.8.2.3), this impressive sensitivity may be even further enhanced.

Since the attainable signal is proportional to the fluorescence collection efficiency δ, it is important to design collection optics with optimum values of δ. Two possible designs are shown in Fig.6.11 which are particularly useful, if the excitation volume is small (e.g., the crossing volume of a laser beam with a collimated molecular beam). One of these collection optics uses a parabolic mirror which collects the light from a solid angle of nearly 2π.

A lens images the light source onto the photomultiplier cathode. The design of Fig.6.11b uses an elliptical mirror where the light source is placed in one focal point A and the polished end of a multifiber bundle into the other B. A half-sphere reflector with its center in A reflects light, which is emitted into the lower halfspace back into the source A which is then further reflected by the elliptical mirror and focussed into B.

The exit end of the fiber bundle can be arranged to have a rectangular shape in order to match it to the entrance slit of a spectrograph (Fig.6.11c).

When the laser wavelength λ_L is tuned across the spectral range of the absorption lines, the total fluorescence intensity $I_{Fl}(\lambda_L) \propto n_L \sigma_{ik} N_i$ monitored as a function of laser wavelength λ_L, represents an image of the absorption spectrum, called the *excitation spectrum*. According to (6.22) the photoelectron rate n_{PE} is directly proportional to the absorption coefficient $N_i \sigma_{ik}$, where the proportionality factor depends on the quantum efficiency η_{ph} of the photo-multiplier cathode and on the collection efficiency δ of the fluorescence photons.

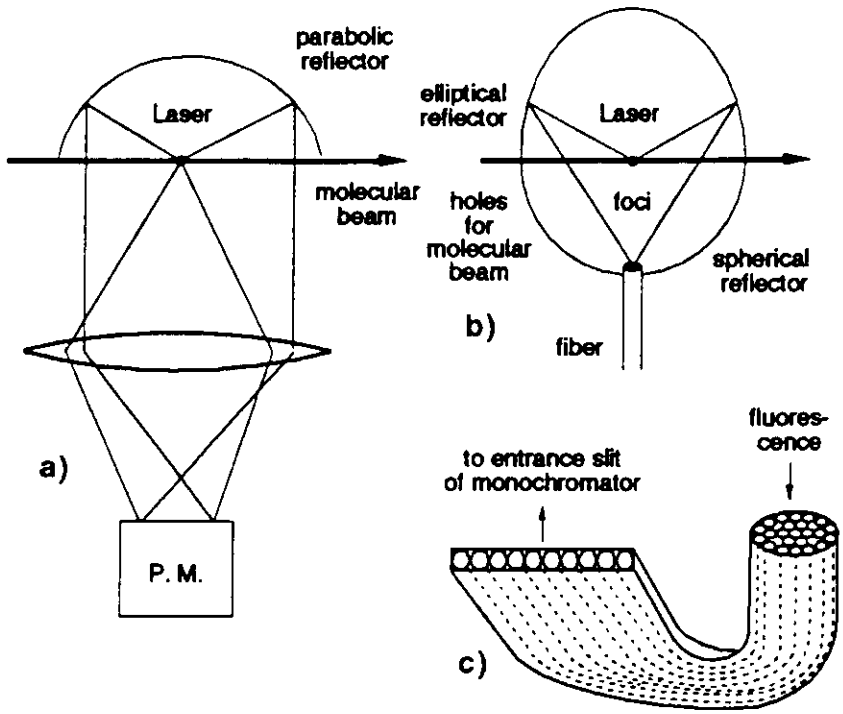

Fig.6.11. (a) Parabolic optical system and (b) elliptical/spherical mirror system with high collection efficiency of fluorescence light. (c) Imaging of the fluorescence onto the entrance slit of a monochromator with a properly adjusted shape of the fibre bundle

Although the excitation spectrum directly reflects the absorption spectrum with respect to the line positions, the relative *intensities* of different lines $I(\lambda)$ are identical in both spectra only if the following conditions are guaranteed:

- The quantum efficiency η_k must be the same for all excited states E_k. Under collision-free conditions, i.e., at sufficiently low pressures, the excited molecules radiate before they can collide, and we obtain $\eta_k = 1$ for all levels E_k.
- The quantum efficiency η_{Ph} of the detector should be constant over the whole spectral range of the emitted fluorescence. Otherwise the spectral distribution of the fluorescence, which may be different for different excited levels E_k, will influence the signal rate. Some modern photomultipliers can meet this requirement.
- The geometrical collection efficiency δ of the detection system should be identical for the fluroescence from different excited levels. This demand excludes, for examples, excited levels with very long lifetimes, where the excited molecules may diffuse out of the observation region before they emit the fluorscence photon. Furthermore, the fluorescence may not be isotropic, depending on the symmetry of the excited state. In this case δ will vary for different upper levels.

However, even if these requirements are not strictly fulfilled, excitation spectroscopy is still very useful, to measure absorption lines with extremely high sensitivity, although their relative intensities may not be recorded accurately.

Example 6.6

With $\Delta x = 0.1$ cm, $\delta = 0.5$, $\eta = 1$ a density $N_i = 10^7/cm^3$ of absorbing molecules yields for an absorption cross section $\sigma_{ik} = 10^{-17}$ cm^2 and an incident flux of $n_L = 10^{16}$ photons/s ($\hat{=}$ 3mW at $\lambda = 500$nm) about $5 \cdot 10^4$ fluorescence photons imaged onto the photomultiplier cathode which emits about $1 \cdot 10^4$ photoelectrons per second.

The LIF method is illustrated by Fig.6.12, which shows a section of the excitation spectrum of Ag_2, taken in a collimated molecular beam under conditions comparable to that of Example 6.6.

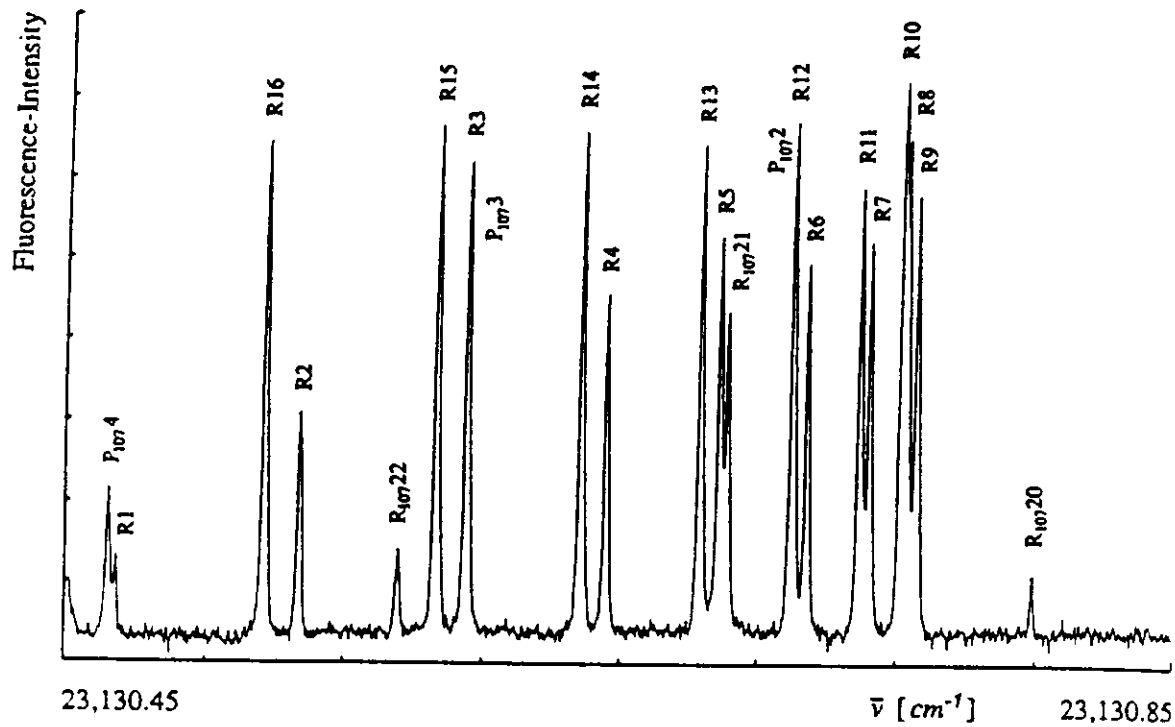

Fig.6.12. Section of the fluorescence excitation spectrum of the $^{107}Ag^{109}Ag$ isotope, showing the band head of the $v' = 1 \leftarrow v'' = 0$ band in the $A^1\Sigma_u \leftarrow X^1\Sigma_g$ system, superimposed by some lines of the $^{107}Ag^{107}Ag$ isotope [6.29]

If in atoms a transition $|i\rangle \rightarrow |k\rangle$ can be selected which represents a true two level system (i.e., the fluorescence from $|k\rangle$ terminates only in $|i\rangle$), the atom may be excited many times while it flies through the laser beam. At a spontaneous lifetime τ and a travel time T a maximum of $n = T/(2\tau)$ excitation-fluorescence cycles can be achieved (photon burst). With $T = 10^{-5}$ s and $\tau = 10^{-8}$ s we can expect $n \hat{=} 500$ fluorescence photons per atom!

4.4 Ionization Spectroscopy

Ionization spectroscopy monitors the absorption of photons on the molecular transition $E_i \rightarrow E_k$ by detecting the ions or electrons, produced by some means, while the molecule is in its excited state E_k.

4.4.1 Basic Techniques

The necessary ionization of the excited molecule may be performed by photons, by collisions, or by an external electric field:

a) Photoionization

The excited molecules can be ionized by absorption of a second photon, i.e.,

$$M^*(E_k) + h\nu_2 \rightarrow M^+ + e^- + E_{kin} \ . \qquad (6.30a)$$

The ionizing photon may come either from the same laser which has excited the level E_k or from a separate light source, which can be another laser or even an incoherent source (Fig.6.19a).

A very efficient photionization process is the excitation of high-lying Rydberg levels above the ionization limit (Fig.6.19b) which decay by autoionization into lower levels of the ion M^+

$$M^*(E_k) + h\nu_2 \rightarrow M^{**} \rightarrow M^+ + e^- + E_{kin} \ . \qquad (6.30b)$$

The absorption cross-section for this process is generally much larger than that of the "bound-free transition" described by (6.30a) (Sect.10.4.2).

The excited molecule may also be ionized by a nonresonant two-photon process (Fig.6.19c)

$$M^*(E_k) + 2h\nu_2 \rightarrow M^+ + e^- + E_{kin} \ . \qquad (6.30c)$$

b) Collision-Induced Ionization

Ionizing collisions between excited atoms or molecules and electrons represent the main ionization process in gas discharges.

$$M^*(E_k) + e^- \rightarrow M^+ + 2e^- \ . \qquad (6.31a)$$

If the excited level E_k is not too far from the ionization limit, the molecule may also be ionized by thermal collisions with other atoms or molecules. If E_k lies above the ionization limit of the collision partners A, Penning ionization [6.57] becomes an efficient process which proceeds as

$$M^*(E_k) + A \rightarrow M + A^+ + e^- \ . \qquad (6.31b)$$

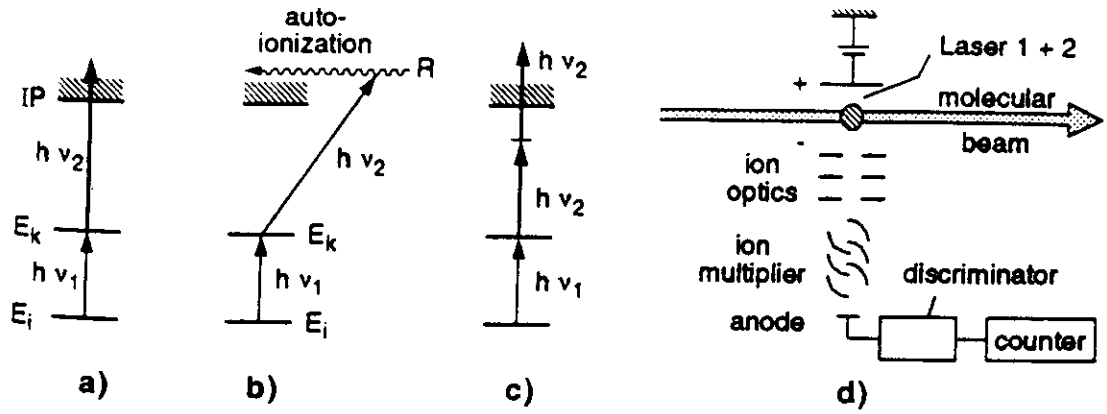

Fig.6.19a-d. Level schemes of ionization spectroscopy. (a) Photo-ionization, (b) excitation of auto-ionizing Rydberg levels, (c) two-photon ionization of excited molecules, (d) experimental arrangement for photoionization spectroscopy in a molecular beam

c) Field Ionization

If the excited level E_k lies closely below the ionization limit, the molecule $M^*(E_k)$ can be ionized by an external electric DC field (Fig.6.20a). This method is particularly efficient if the excited level is a long-lived highly excited Rydberg state. The required minimum electric field can readily be estimated from Bohr's atomic model, which gives a good approximation for atomic levels with large principal quantum number n. The ionization potential for the outer electron at the mean radius r from the nucleus is determined by the Coulomb field of the nucleus shielded by the inner electron core.

$$IP = \int_r^\infty \frac{Z_{eff}\, e^2}{4\pi\epsilon_0 r^2} dr = \frac{Z_{eff}\, e^2}{4\pi\epsilon_0\, r}$$

where eZ_{eff} is the effective nuclear charge, i.e. the nuclear charge eZ partly screened by the electron cloud. If an external field $E_{ext} = -E_0 x$ is applied, the effective ionization potential is lowered to the value

$$IP_{eff} = IP - \sqrt{\frac{Z_{eff}\, e^3 E_0}{\pi\epsilon_0}} \,. \qquad (6.32)$$

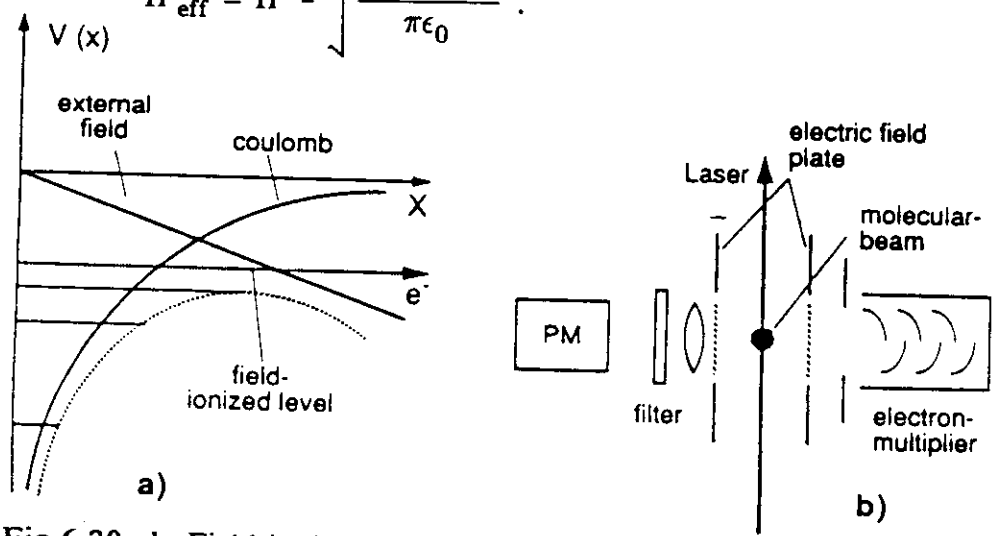

Fig.6.20a,b. Field ionization of highly excited levels closely below the ionization limit: (a) Potential diagram and (b) experimental arrangement for field ionization in a molecular beam. The photomultiplier monitors the LIF from the intermediate level populated in a two-step excitation process

If the energy E of the excited level is above IP_{eff}, it will be field-ionized.

Techniques, where the laser excites the atoms, but the ionizing step is performed by field ionization, have found increasing applications in the detection of Rydberg atoms in molecular beams (Sect.14.6), in analytical chemistry for trace elements or small concentrations of pollutants [6.58].

Example 6.9

For levels 10 meV below the ionization limit, (6.32) gives $E_0 \geq 1.7 \cdot 10^4$ V/m for the ionizing external field. However, because of the quantum-mechanical tunnel effect the fields required for complete ionization are even lower.

4.4.2 Sensitivity of Ionization Spectroscopy

The following estimation illustrates the possible sensitivity of ionization spectroscopy (Fig.6.19a). Let N_k be the density of excited molecules in level E_k, P_{kI} the probability per second that a molecule in level E_k is ionized, and n_a the number of photons absorbed per second on the transition $E_i \rightarrow E_k$. If R_k is the total relaxation rate of level E_k, besides the ionization rate (spontaneous transitions plus collision-induced deactivation) the signal rate in counts per second is for the absorption path length Δx and for n_L incident laser photons per second:

$$S_I = N_k P_{kI} \delta \cdot \eta = n_a \frac{P_{kI}}{P_{kI} + R_k} \delta \cdot \eta = N_i n_L \sigma_{ik} \Delta x \frac{P_{kI}}{P_{kI} + R_k} \delta \cdot \eta \,. \qquad (6.33)$$

With a proper design the *collection* efficiency δ for the ionized electrons or ions can reach $\delta = 1$. If the electrons or ions are accelerated to several keV and detected by electron multipliers or channeltrons a *detection* efficiency of $\eta = 1$ can be achieved, too. If the ionization probability P_{kI} can be made large compared to the relaxation rate R_k of the level $|k\rangle$ the signal S_I then becomes with $\delta = \eta = 1$:

$$S_I \sim n_a \,.$$

This means that every laser photon absorbed in the transition $E_i \rightarrow E_k$ gives rise to a detected ion or electron. It implies that *single absorbed photons* can be detected with an overall efficiency close to unity (or 100%). In experimental practice there are, of course, additional losses and sources of noise, which limit the detection efficiency to a somewhat lower level. However, for all absorbing transitions $E_i \rightarrow E_k$, where the upper level E_k can readily be ionized, ionization spectroscopy is the most sensitive detection technique and superior to all other methods discussed so far [6.59, 60].

4.4.3 Pulsed vs CW Lasers for Photoionization

In case of photoionization of the excited level $|k\rangle$ the ionization probability per second

$$P_{kI} = \sigma_{kI}\, n_{L_2} \quad [s^{-1}]$$

equals the product of the ionization cross section σ_{kI} [cm^2] and the photon flux density n_{L_2} [$cm^{-2} \cdot s^{-1}$] of the ionizing laser. We can then write (6.33) as

$$S_I = N_i \left[\frac{\sigma_{ik}\, n_{L_1}\, \delta \cdot \eta}{1 + R_k/(\sigma_{kI}\, n_{L_2})} \right] \Delta x \,. \tag{6.34}$$

The maximum ion rate S_I^{max} which is achieved if

$$\sigma_{kI}\, n_{L2} >> R_k$$

becomes equal to the rate n_a of photons absorbed in the transition $|i\rangle \rightarrow |k\rangle$:

$$S_I^{max} = N_i \sigma_{ik}\, n_{L_1}\, \Delta x = n_a \,. \tag{6.35}$$

The following estimation illustrates whether this maximum ion rate can be realized: Typical cross sections for photoionization are $\sigma_{kI} \sim 10^{-17}$ cm^2. If radiative decay is the only deactivation mechanism of the excited level $|k\rangle$ we have $R_k = A_k \approx 10^8$ s^{-1}. In order to achieve $n_{L_2}\, \sigma_{kI} > A_k$ we need a photon flux $n_{L_2} > 10^{25}$ $cm^{-2} \cdot s^{-1}$ of the ionizing laser. With pulsed lasers this condition can be met readily.

Example 6.10

Excimer laser: 100 mJ/pulse, ΔT = 10 ns, the cross section of the laser beam may be 1 $cm^2 \rightarrow n_{L2} = 2 \cdot 10^{25}$ $cm^{-2} \cdot s^{-1}$. With the numbers above we can reach an ionization probability of $P_{ik} = 2 \cdot 10^8$ s^{-1} for all molecules within the laser beam. This gives an ion rate S_I which is 2/3 of the maximum rate $S_I = n_a$.

The advantage of pulsed lasers is the large photon flux during the pulse time ΔT which allows the ionization of the excited molecules *before they decay* by relaxation into lower levels where they are lost for further ionization. Their disadvantages are their large spectral bandwidth that is generally larger than the Fourier-limited bandwidth $\Delta\nu \geq 1/\Delta T$ and their low duty cycle. At typical repetition rates of f_L = 10 to 100 s^{-1} and a pulse duration of $\Delta T = 10^{-8}$ s the duty cycle is only 10^{-7} - 10^{-6}!

If the diffusion time t_D of molecules out of the excitation-ionization region is smaller than $1/f_L$, at most the fraction $f_L t_D$ of molecules can be ionized, even if the ionization probability during the laser pulse ΔT approaches 100%.

Example 6.11

Assume that the two laser beams L1 and L2 for excitation and ionization have the diameter D = 1 cm and traverse a collimated molecular beam with 1 cm^2 cross section perpendicularly. During the pulse time $\Delta T = 10^{-8}$ s the distance, travelled by the molecules at the mean velocity $\bar{v} = 500$ m/s is $d = \Delta T \bar{v} \sim 5 \cdot 10^{-4}$ cm. This means that all molecules in the excitation volume of 1 cm^3 can be ionized during the time ΔT. During the "dark" time $T = 1/f_L$, however, the molecules travel the distance $d = \bar{v}T \sim 500$ cm at $f_L = 10^2\ s^{-1}$. Therefore, only the fraction $1/500 = 2 \cdot 10^{-3}$ of all molecules in the absorbing level $|i\rangle$ are ionized in a continuous molecular beam.

There are two solutions:

(i) If pulsed molecular beams can be employed having the pulse time $\Delta T_B \leq D/\bar{v}$ and the repetition rate $f_B = f_L$, an optimum detection probability can be achieved.

(ii) In continuous molecular beams the two laser beams may propagate antiparallel to the molecular-beam axis. If lasers with a high-repetition frequency f_L are used (for example, copper-laser-pumped dye lasers with $f_L \leq 10^4 s^{-1}$), then the distance travelled by the molecules during the dark time is only $d = \bar{v}/f \geq 5$ cm. They can therefore still be detected by the next pulse [6.61,62].

With CW lasers the duty cycle is 100% and the spectral resolution is not limited by the laser bandwidth. However, the laser beam has to be focussed in order to meet the requirement $P_{kI} > R_k$.

Example 6.12

If a CW argon laser with 10 W at $\lambda = 488$ nm ($\hat{=} 2.5 \cdot 10^{19}$ photon/s) is used for the ionizing step, it has to be focussed down to an area of $1.5 \cdot 10^{-6}$ cm^2, i.e. a diameter of 10 μm in order to reach a photon flux density of $n_{L2} = 10^{25}\ cm^{-2} \cdot s^{-1}$.

Here the following problem arises: The molecules excited by laser L1 into level $|k\rangle$ travel during their spontaneous lifetime of $\tau = 10$ ns at the thermal velocities $\bar{v} = 5 \cdot 10^4$ m/s only a distance of $d = 5$ μm before they decay into lower levels. The second laser L2 has therefore to be focussed in a similar way as L1 and its focus has to overlap that of L1 within a few μm.

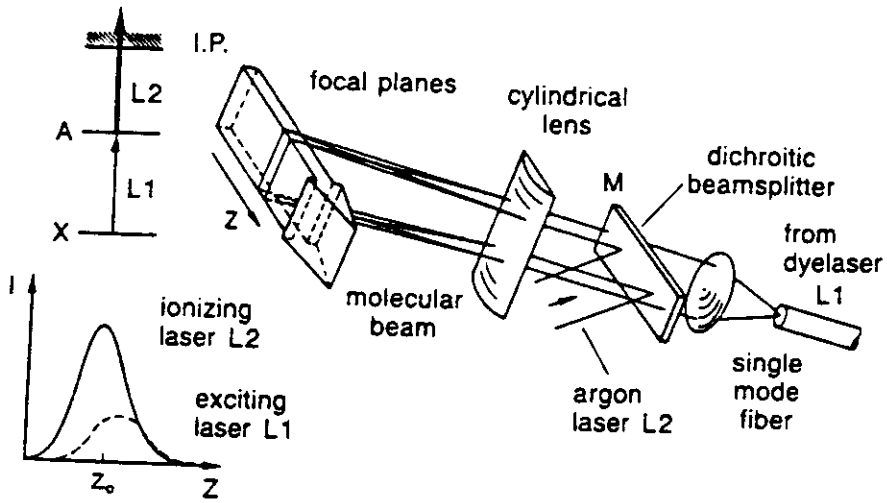

Fig.6.21. Experimental arrangement for resonant two-photon two-colour ionization with two CW lasers. The insert shows the optimum overlap of the Gaussian intensity profiles in the focal plane

A technical solution of this problem is depicted in Fig.6.21. The dye laser L1 is guided through a single-mode optical fiber. The divergent light, emitted out of the fiber end is made parallel by a spherical lens, superimposed with the beam of the argon laser L2 by a dichroic mirror M. Both beams are then focussed by a cylindrical lens into the molecular beam, forming there a rectangular "sheet of light" with a thickness of about $5 \div 10$ μm and a height of about 1 mm, adapted to the dimensions of the molecular beam [6.63]. All molecules in the beam have to pass through the two laser beams. Since the transition probability for the first step $|i\rangle \rightarrow |k\rangle$ is generally larger by some orders of magnitude than that of the ionizing transition, the first transition can be readily saturated (Sect.7.1). It is therefore advantageous, to adjust the relative positions of the two beams in such a way, that the maximum intensity of L2 coincides spatially with the slope of the Gaussian intensity profile of L1 (see insert of Fig.6.21).

Often it is possible to tune the ionizing laser L2 to transitions from $|k\rangle$ into autoionizing Rydberg levels (Sect.10.4). For such transitions the probability may be $2 \div 3$ orders of magnitude larger than for bound-free transitions into the ionization continuum. In these cases the requirement (6.35) can be met already at much lower intensities of L2.

The resonant two-step ionization with two laser photons from pulsed or CW lasers represents the most versatile and sensitive detection technique. If laser L1 excites all atoms or molecules which fly through the laser beam, single atoms or molecules can be detected [6.59, 64, 65] if the condition (6.35) can be fulfilled.

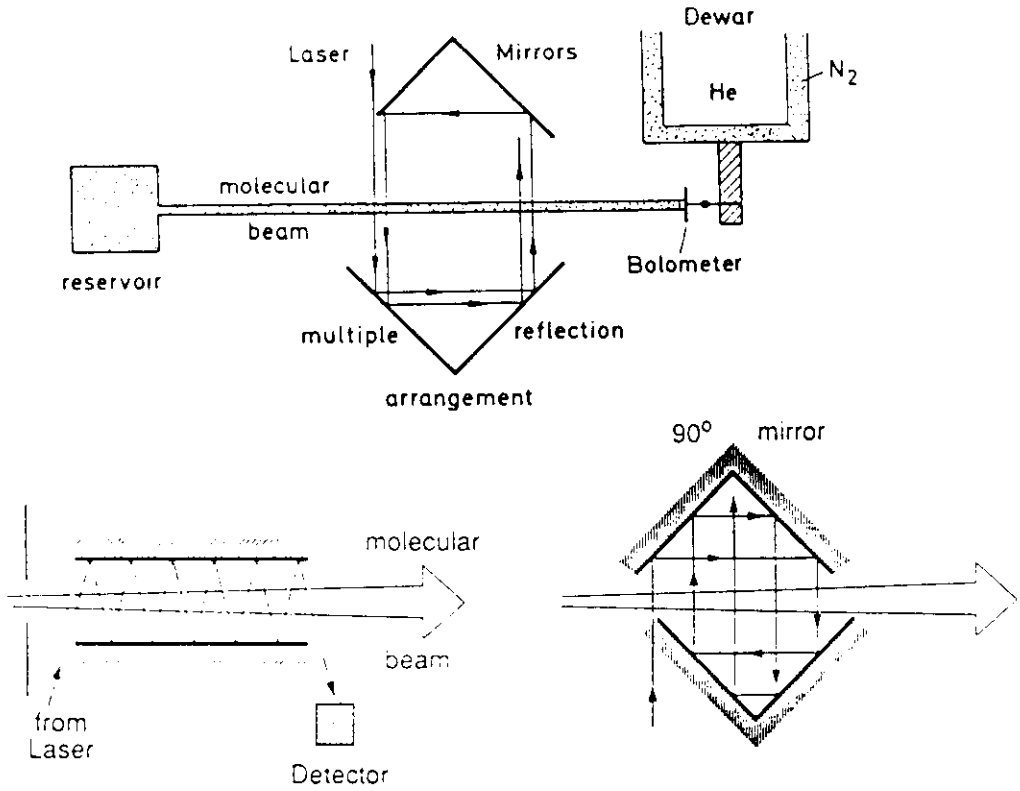

Fig.6.16. Optothermal spectroscopy in a molecular beam with a helium-cooled bolometer as detector and two optical systems which increase the absorption path length

6.3.3 Optothermal Spectroscopy

For the spectroscopy of vibrational-rotational transitions in molecules the laser-excited fluorescence is generally not the most sensitive tool, as has been discussed at the end of Sect.6.3.1. The optoacoustic spectroscopy, on the other hand, is based on collisional energy transfer and is therefore not applicable to molecular beams, where collisions are rare or even completely absent. For the infrared spectroscopy of molecules in a molecular beam therefore a new detection technique has been developed, which relies on the collision-free conditions in a beam and on the long radiative lifetimes of vibrational-rotational levels in the electronic ground state [6.52].

Optothermal spectroscopy uses a cooled bolometer (Sect.4.5) to detect the excitation of molecules in a beam (Fig.6.16). When the molecules hit the bolometer they transfer their kinetic and their internal thermal energy thereby increasing the bolometer temperature to a stationary value T. If the molecules are excited by a tunable laser (for example, a colour-center laser or a diode laser) their vibrational-rotational energy increases by $\Delta E = h\nu$. If the lifetime τ of the excited levels is larger than the flight time $t = d/v$ from the excitation region to the bolometer, they transfer this extra energy to the bolometer. If N excited molecules hit the bolometer per second, the rate of heat transfer is

$$\frac{dQ}{dt} = N\Delta E = Nh\nu \, . \qquad (6.27)$$

With the heat capacity C of the bolometer and a heat conduction $G(T-T_0)$ the temperature T is determined by

$$N h\nu = C \frac{dT}{dt} + G(T-T_0) . \tag{6.28}$$

Under stationary conditions ($dT/dt = 0$) we obtain from (6.28) the temperature rise

$$\Delta T = T - T_0 = \frac{N h\nu}{G} . \tag{6.29}$$

In general, the exciting laser beam is chopped in order to increase the signal/noise ratio by lock-in detection. The time constant $\tau = C/G$ of the bolometer (Sect.4.5) should be smaller than the chopping period. One therefore has to construct the bolometer in such a way that both C and G are as small as possible.

The temperature change ΔT can be measured by the resulting resistance change

$$\Delta R = \frac{dR}{dT} \Delta T$$

which is a function of the temperature dependence dR/dT of the bolometer material. Large values of dR/dT are achieved with semiconductor materials at low temperatures (a few Kelvin!). Even larger values can be realized with materials around their critical temperature T_c for the transition from the superconducting to the normal conducting state. In this case, however, one always has to keep the temperature at T_c. This can be achieved by a temperature feedback control where the feedback signal is a measure for the rate dQ/dt of energy transfer to the bolometer by the excited molecules.

With such a detector at T = 4 K energy transfer rates $dQ/dt \geq 10^{-12}$ W are still detectable [6.53]. This means that an absorbed laser power of $\Delta P \geq 10^{-12}$ W is measurable. In order to maximize the absorbed power, the absorption path length can be increased by an optical device consisting of two 90° reflectors which reflect the laser beam many times back and forth through the molecular beam (Fig.6.16).

The sensitivity of the optothermal technique is illustrated by the infrared spectrum of a vibrational-rotational transition of the NO molecule with fully resolved hyperfine structure (Fig.6.17). This has been measured with a colour center laser crossed with a collimated NO beam [6.54].

The term "photothermal spectroscopy" is also used in the literature for the generation of thermal-wave phenomena in samples which are illuminated with a time-dependent light intensity [6.55]. In many aspects this is equivalent to photo-acoustic spectroscopy. An interesting modification of this technique for the study of molecules adsorbed at surfaces, is illustrated in Fig.6.18. A small spot of a surface is irradiated by a pulsed-laser beam.

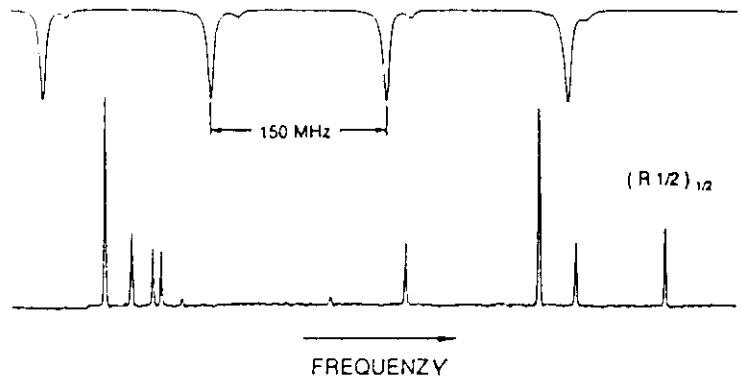

Fig.6.17. Vibration-rotation transition ($v = 0 \rightarrow 2$; $J = 1/2 \rightarrow 3/2$) with resolved hyperfine structure of the NO molecule, measured with optothermal spectroscopy in a collimated molecular beam [6.54]

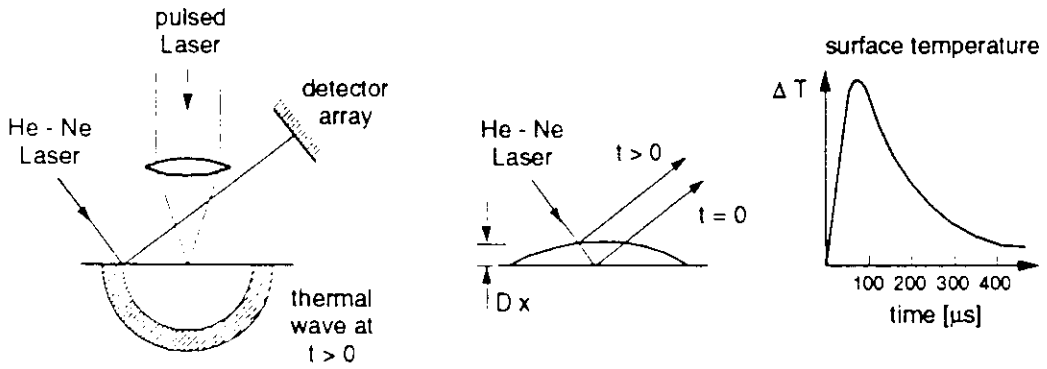

Fig.6.18a-c. Optothermal spectroscopy of solids and of molecules adsorbed at surfaces. (a) Propagation of thermal wave induced by a pulsed laser. (b) Deformation of a surface detected by the deflection of a HeNe laser beam. (c) Time profile of surface temperature change following pulsed illumination [6.56]

The absorbed power results in a temperature rise of the illuminated spot. This temperature will travel as a thermal shock wave through the solid. It leads to a slight time-dependent deformation of the surface, due to thermal expansion. This deformation is probed by the time-dependent deflection of a low-power HeNe laser. In case of adsorbed molecules the absorbed power varies when the laser wavelength is tuned over the absorption spectrum of the molecules. Time-resolved measurements of the probe-beam deflection allows one to determine the kind and amount of adsorbed molecules and to follow up their desorption with time, caused by the irradiating light [6.56].

15.5 Medical Applications of Laser Spectroscopy

Numerous books have meanwhile been published on laser applications in medical research in hospital practice [15.115-118]. Most of these applications rely on the high laser-output power which can be focussed into a small volume. The strong dependence of the absorption coefficient of living tissue on the wavelength allows selection of the penetration depth of the laser beam by choosing the proper laser wavelength [15.117]. For example, skin carcinoma or portwine marks should be treated at wavelengths for a small penetration depth in order to protect the deeper layers of the epidermia from being damaged, while cutting of bones with lasers or treatment of subcutan cancer must be performed at wavelengths with greater penetration depth. The most spectacular outcomes of laser applications in medicine have been achieved in laser surgery, dermatology, opthalmology and dentistry.

There are, however, also very promising direct applications of laser *spectroscopy* for the solution of problems in medicine. They are based on new diagnostic techniques. Some of them are discussed in this section.

15.5.1 Applications of Raman Spectroscopy in Medicine

During the operation of a patient, the optimum concentration and composition of narcotic gases can be indicated by the composition of the respiratory gases, i.e. with the concentration ratio of $N_2:O_2:CO_2$. This ratio can be measured in vivo with Raman spectroscopy [15.119]. The gas flows through a cell which is placed inside a multipass arrangement for an argon-laser beam (Fig.15.21). In a plane perpendicular to the beam axis several detectors with special spectral filters are arranged. Each detector monitors a selected Raman line which allows the simultaneous detection of all molecular components of the gas.

The sensitivity of the method is illustrated by Fig.15.22, which depicts the time variation of the CO_2, O_2 and N_2 concentration in the exhaled air of a human patient. Note the variation of the concentrations with changing breathing period. The technique can be used routinely in clinical practice for anesthetic control during operations and obviously also for alcohol tests of car drivers.

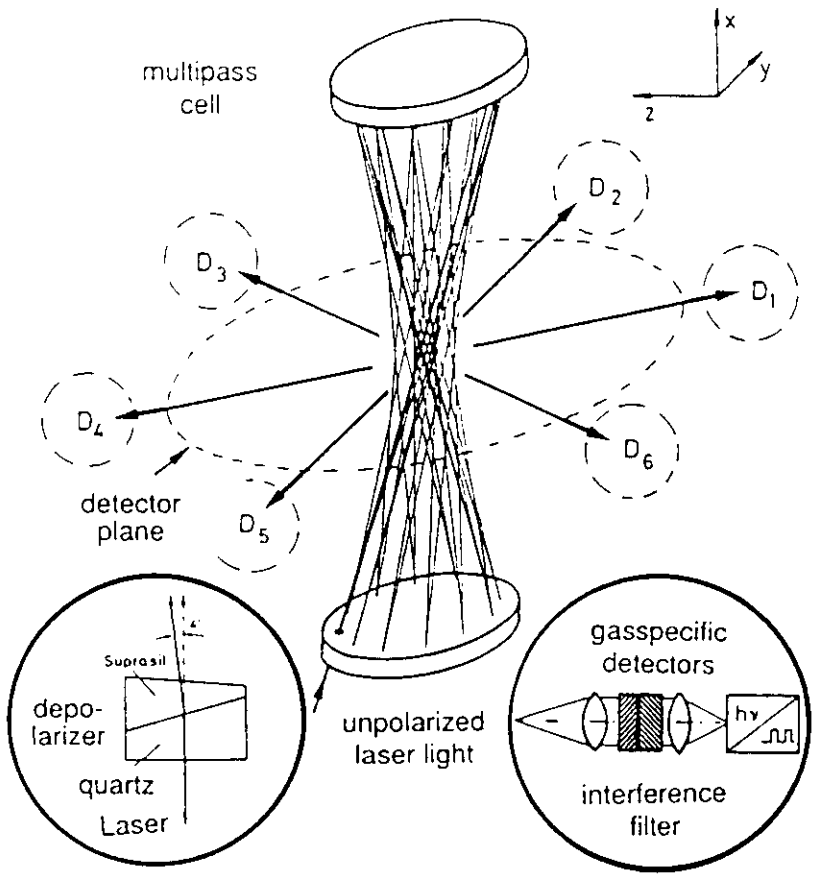

Fig.15.21. Multipass cell and spectrally selective detector arrangement for sensitive Raman spectroscopy and diagnostics of molecular gases [15.119]

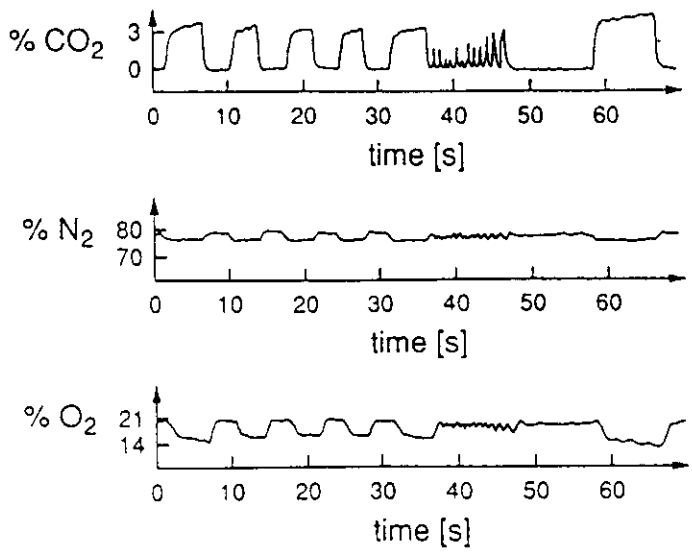

Fig.15.22. CO_2, N_2 and O_2 concentrations of respiratory gases for varying breath periods, measured in vivo with the arrangement of Fig.15.22 [15.119]

15.5.2 Heterodyne Measurements of Ear Drums

A large fraction of ear diseases of elderly people is due to changes in the frequency response of the ear drum. While up to now investigations of such changes had to rely on the subjective response of the patient, novel laser-spectroscopy techniques allow objective studies of frequency-dependent vibrational amplitudes of the ear drum and their local variation for different locations on the drum with a laser Doppler vibrometer (Fig. 15.23). The experimental arrangement is illustrated in Fig. 15.24. The output of a diode laser is fed through an optical fiber to the ear drum. The light reflected by the drum is collected by a lens at the end of the fiber and is sent back through the fiber where it is superimposed on a photodetector behind a beam splitter with part of the direct laser light. The ear is exposed to the

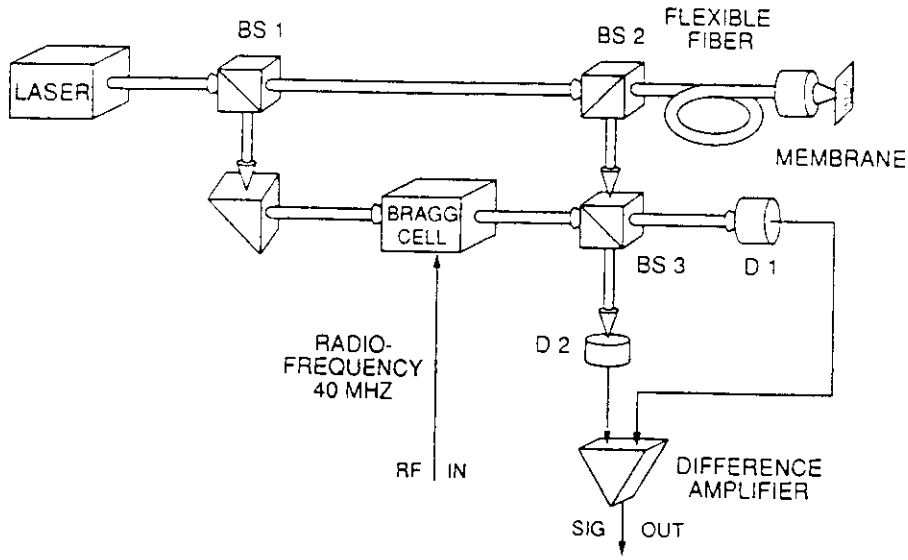

Fig. 15.23. Principle of laser Doppler vibrometer

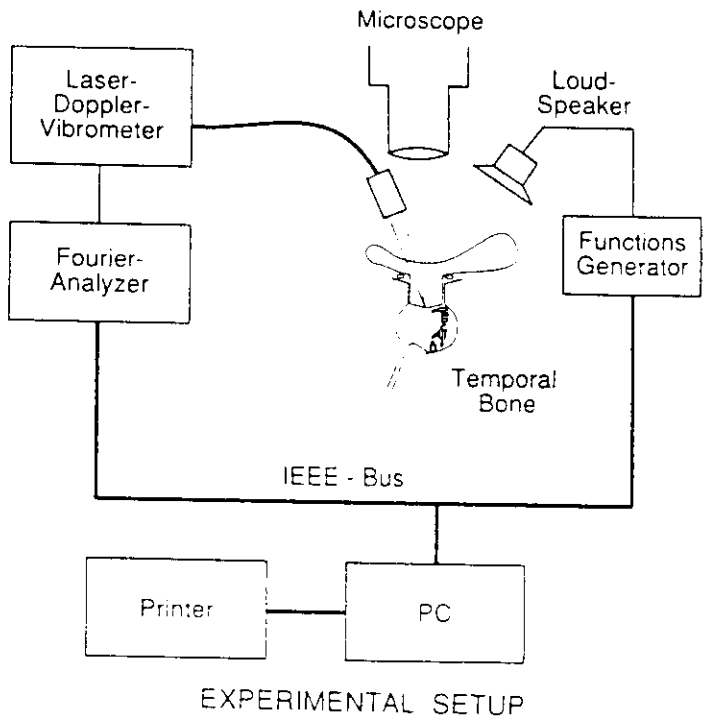

EXPERIMENTAL SETUP

Fig. 15.24. Heterodyne measurements of frequency-dependent vibrations of the ear drum and their local variations

sound waves of a loudspeaker with variable audio frequency f. The frequency ω of the light reflected by the vibrating ear drum is Doppler shifted. From the frequency spectrum of the heterodyne signals the amplitude A(f) of the illuminated area of the vibrating drum can be derived (Sect.12.6). In order to transfer the heterodyne spectrum in a region with less noise, the laser light is modulated at the frequency $\Omega \approx 40$ MHz by an opto-acoustic modulator producing sidebands at $\omega \pm \Omega$ [15.120].

15.5.3 Cancer Diagnostics and Therapy with the HPD Technique

Recently, a method for diagnostics and treatment of cancer has been developed which is based on photoexcitation of the fluorescing substance HematoPorphyrin Derivate (HPD) [15.121]. A solution of this substance is injected into the veins and is distributed in the whole body after a few hours. While HPD is released by normal cells after 2÷4 days it is kept by cancer cells for a longer time [15.122]. If a tissue containing HPD is irradiated by a UV laser, it emits a characteristic fluorescence spectrum which can be used for a diagnostic of cancer cells. Figure 15.25 shows the emission spectrum of a tissue with and without HPD, and also the fluorescence of pure HPD in a liquid solution excited by a nitrogen laser at $\lambda = 337$ nm. The experimental arrangement for detecting a cancerous tissue in rats is exhibited in Fig.15.26 [15.123]. The fluorescence is spectrally resolved by a grating and spatially separated by three slightly folded mirrors which image a cancer region and a region of normal cells onto different parts of the diode array of an optical multichannel analyser (Sect.4.5). A computer subtracts the fluorescence of the normal tissue from that of a cancerous tissue.

Absorption of photons in the range 620÷640 nm brings HPD into an excited state, which reacts with normal oxygen in the $O_2(^3\Pi)$ state and transfer it into the $O_2(^1\Delta)$ state which apparently reacts with the surrounding cells and destroys them. Although the exact mechanism of these processes is not yet completely understood, it seems that this HPD method allows a rather selective destruction of cancer cells without too much damage to the normal cells. The technique was developed in the USA, intensively applied in Japan [15.124] and has meanwhile been applied successfully to patients with oesophagus cancer, cervix carcinoma and other kinds of tumors which can be reached by optical fibers without invasive surgery [15.125].

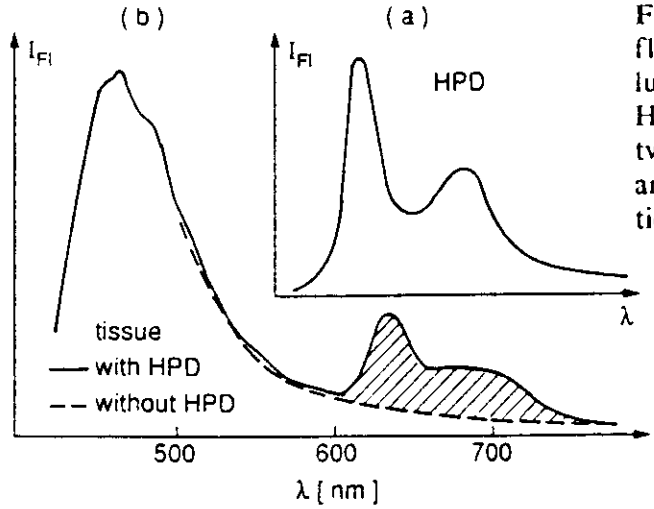

Fig.15.25. Nitrogen-laser-excited fluorescence spectrum of HPD in solution (**a**) and of tissue (**b**) without HPD (*dashed curve*), and with HPD two days after injection. The hatched area represents the additional absorption of HPD [15.123]

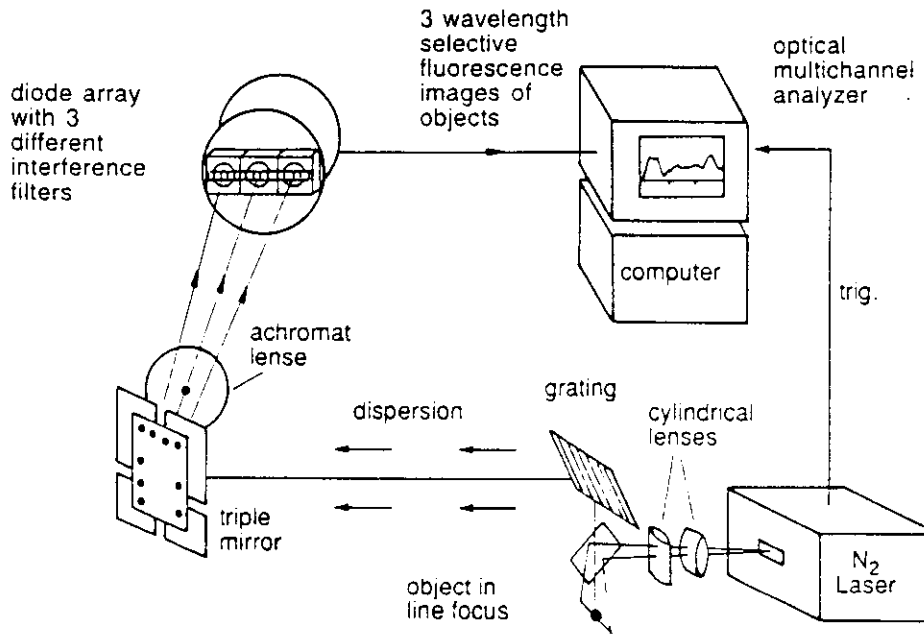

Fig.15.26. Experimental arrangement for cancer diagnostics of rat tissue [15.123]

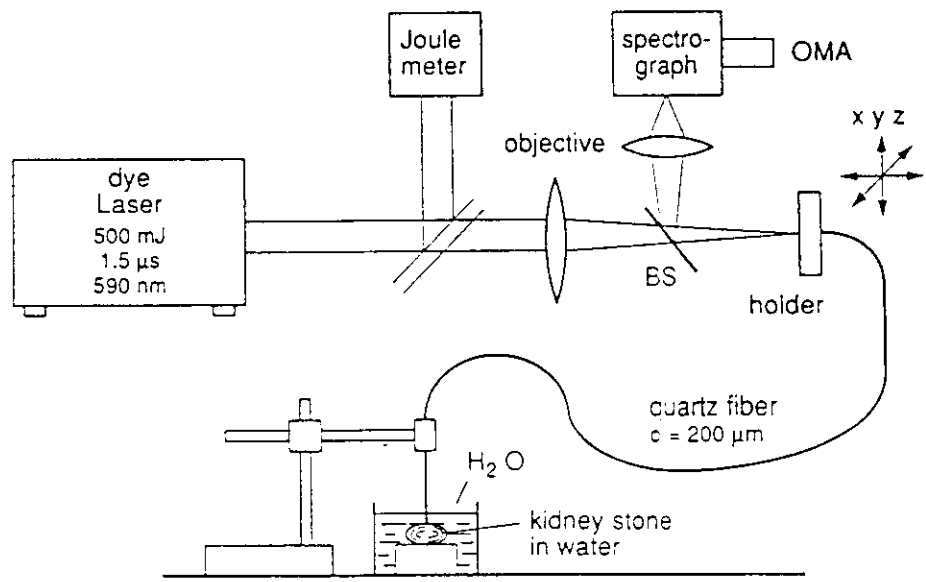

Fig.15.27. Experimental arrangement for the spectral analysis of kidney stones for the determination of stone composition

15.5.4 Laser Lithotripsy

Due to the development of thin, flexible optical fibers with a high damage threshold for the laser radiation [15.126, 127], inner organs of the human body, such as stomach, bladder, gall or kidneys, can be selectively irradiated by laser radiation. A new technique of breaking gall stones to pieces by irradiation with pulsed lasers (laser lithotripsy) has found increasing interest because it has several advantages compared to the ultrasonic shock-wave lithotripsy [15.128, 129].

The optical fiber of fused quartz is inserted through the urinary channel until it nearly touches the stone that is to be broken. This can be monitored by X-Ray diagnosis or by endoscopy through a fiber bundle which contains, besides the fiber for guiding the laser beam, other fibers for illumination, viewing and monitoring the laser-induced fluorescence.

If the pulse of a flashlamp-pumped dye laser is transported through the fiber and focussed onto the gall stone, the rapid evaporation of the stone material results in a shock wave in the surrounding liquid which leads to a destruction of the stone after several laser shots [15.129]. The necessary laser power and the optimum wavelength depend on the chemical composition of the stone, which generally varies for different patients. It is therefore advantageous to know the stone composition before the distruction in order to choose optimum laser conditions. This information can be obtained by collecting the fluorescence of the evaporated stone material at low laser powers through an optical fiber (Fig. 15.27). The fluorescence spectrum is monitored with an optical multichannel analyser and a computer gives, within seconds, the wanted information about the stone composition [15. 130].

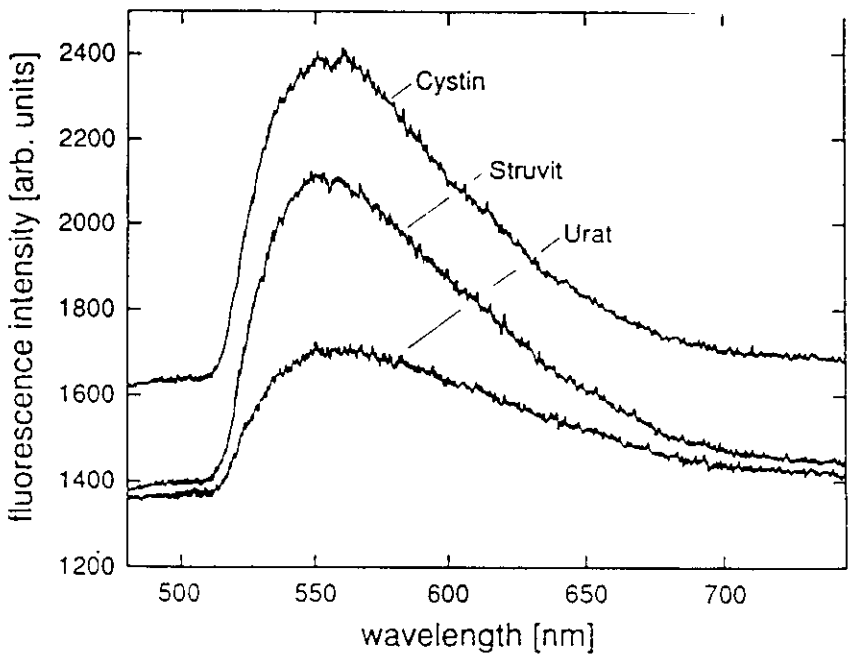

Fig. 15.28. Fluorescence of three different kidney-stone materials excited with a dye laser at λ = 497 nm at low intensities to prevent plasma breakdown [15.131]

First demonstrations of the capability of spectral analysis of kidney stones in vitro are illustrated in Fig. 15.28 where the fluorescence spectra of different kidney stones which had been irradiated in a water surrounding outside the body, and which were detected with the arrangement of Fig. 15.26, are shown [15.131].

Further information on laser lithotripsy and spectroscopic control of this technique can be found in [15.132, 133].

6.31 References to the historical development can be found in H.J. Bauer: Son et lumiere or the optoacoustic effect in multilevel systems. J. Chem. Phys. 57, 3130 (1972)
6.32 Yoh-Han Pao (ed.): *Optoacoustic Spectroscopy and Detection* (Academic, New York 1977)
6.33 A. Rosencwaig: *Photoacoustic and Photoacoustic Spectroscopy* (Wiley, New York 1980)
6.34 V.P. Zharov, V.S. Letokhov: *Laser Optoacoustic Spectroscopy*, Springer Ser. Opt. Sci., Vol. 37 (Springer, Berlin, Heidelberg 1986)
6.35 C. Forbes Dewey, Jr.: Opto-acoustic spectroscopy, in *Impact of Lasers on Spectroscopy*, Proc. Soc. Photo Opt. Instrum. Eng. **49**, 13 (1974)
6.36 C.K.N. Patel: Spectroscopic measurements of stratospheric nitric oxide and water vapor. Science **184**, 1173 (1974)
6.37 A. Rosencwaig: The spectraphone. Anal. Chem. **47**, 592A (1975)
6.38 S.O. Kanstadt, P.E. Nordal: Photoacoustic and photothermal spectroscopy. Phys. Technol. **11**, 142 (1980)
6.39 P. Hess, J. Pelzl (eds.): *Photoacoustic and Photothermal Phenomena*, Springer Ser. Opt. Sci., Vol.58 (Springer, Berlin, Heidelberg 1988)
6.40 P. Hess (ed.): *Photoacoustic, Photothermal and Photochemical Processes in Gases*, Topics Curr. Phys., Vol.46 (Springer, Berlin, Heidelberg 1989)
6.41 J.C. Murphy, J.W. Maclachlan Spicer, L.C. Aamodt, B.S.H. Royce (eds.): *Photoacoustic and Photothermal Phenomena II*, Springer Ser. Opt. Sci., Vol.62 (Springer, Berlin, Heidelberg 1990)
6.42 L.B. Kreutzer: Laser optoacoustic spectroscopy. A new technique of gas analysis. Anal. Chem. **46**, 239A (1974)
6.43 W. Schnell, G. Fischer: Spectraphone measurements of isotopes of water vapor and nitricoxyde and of phosgene at selected wavelengths in the CO- and CO_2-laser region. Opt. Lett. 2, 67 (1978)

6.44 S.D. Smith: High resolution infrared spectroscopy, in *High Resolution Spectroscopy*, ed. by S.D. Smith (Academic, New York 1976) p.13
6.45 Ch. Hornberger, W. Demtröder: Photoacoustic overtone spectroscopy of acethylene in the visible and near infrared. Chem. Phys. Lett. **190**, 171 (1994)
6.46 C.K.N. Patel: Use of vibrational energy transfer for excited-state opto-acoustic spectroscopy of molecules. Phys. Rev. Lett. **40**, 535 (1978)
6.47 G. Stella, J. Gelfand, W.H. Smith: Photoacoustic detection spectroscopy with dye laser excitation. The 6190 Å CH_4 and the 6450 NH_3-bands. Chem. Phys. Lett. **39**, 146 (1976)
6.48 A.M. Angus, E.E. Marinero, M.J. Colles: Opto-acoustic spectroscopy with a visible CW dye laser. Opt. Commun. **14**, 223 (1975)
6.49 E.E. Marinero, M. Stuke: Quartz optoacoustic apparatus for highly corrosive gases. Rev. Sci. Instrum. **50**, 31 (1979)
6.50 A.C. Tam: Photoacoustic, Spectroscopy and other applications. In *Ultrasensitive Laser Spectroscopy*, ed. by D.S. Kliger (Academic, New York 1983) pp.1-108
6.51 A.C.Tam, C.K.N. Patel: High-resolution optoacoustic spectroscopy of rare-earth oxide powders. Appl. Phys. Lett. **35**, 843 (1979)
6.52 T.E. Gough, G. Scoles: Optothermal infrared spectroscopy, in *Laser Spectroscopy V*, ed. by A.R.W. McKeller, T. Oka, B.P. Stoicheff, Springer Ser. Opt. Sci., Vol.30 (Springer, Berlin, Heidelberg 1981) p.337
6.53 M. Zen: Cyrogenic bolometers, in *Atomic and Molecular Beams Methods* (Oxford Univ. Press, London 1988) Vol.1
6.54 R.E. Miller: Infrared laser spectroscopy of molecular beams. PhD Thesis, Univ. of Waterloo, Ontario (1980)
6.55 H. Coufal: Photothermal spectroscopy and its analytical application. Fresenius Z. Anal. Chem. 337, 835 (1990)
6.56 F. Träger: Surface analysis by laser-induced thermal waves. Laser u. Optoelek-

15.115 L. Goldstein (ed.): *Laser Non-Surgical Medicine. New Challenges for an Old Application* (Lancaster, Basel 1991)
15.116 G. Biamino, G. Müller (eds.): *Advances in Laser Medicine I* (Ecomed. Verlagsgesell., Berlin 1988)
15.117 St. L. Jacques (ed.): *Proc. Laser Tissue Intersection II.* SPIE Proc. **1425** (1991)
A. Anders, I. Lamprecht, H. Schacter, H. Zacharias: The use of dye lasers for spectroscopic investigations and photodynamics therapy of human skin. Arch. Dermat. Res. 255, 211 (1976)
15.118 H.P. Berlien, G. Müller (eds.): *Angewandte Lasermedizin* (Ecomed. Landsberg 1989)
15.119 H. Albrecht, G. Müller, M. Schaldach: Entwicklung eines Raman-spektroskopisches Gasanalysesystems. Biomed. Tech. 22, 361 (1977)
Proc. VII Int'l Summer School on Quantum Optics, Wiezyca, Poland (1979)
15.120 H.J. Foth, N. Stasche, K. Hörmann: Measuring the motion of the human tympanic membran by laser Doppler vibrometry. SPIE Proc. **2083**, 250-262 (1994)
15.121 T.J. Dougherty, J.E. Kaulmann, A. Goldfarbe, K.R. Weishaupt, D. Boyle, A. Mittleman: Photoradiation therapy for the treatment of malignant tumors. Cancer Res. **38**, 2628 (1978)
D. Kessel: Components of hematoporphyrin derivates and their tumor-localizing capacity. Cancer Res. **42**, 1703 (1982)
15.122 P.J. Bugelski, C.W. Porter, T.J. Dougherty: Autoradiographic distribution of HPD in normal and tumor tissue in the mouse. Cancer Res. **41**, 4606 (1981)
15.123 A.S. Svanberg: Laser spectroscopy applied to energy, environmental and medical research. Phys. Scr. **23**, 281 (1988)
15.124 Y. Hayata, H. Kato, Ch. Konaka, J. Ono, N. Takizawa: Hematoporphyrin derivative and laser photoradiation in the treatment of lung cancer. Chest **81**, 269 (1982)
15.125 A. Katzir: Optical Fibers in Medicine IV. SPIE Proc. **1067** (1989); ibid **906** (1988)
15.126 L. Prause, P. Hering: Lichtleiter für gepulste Laser: Transmissionsverhalten, Dämpfung und Zerstörungsschwellen. Laser Optoelektron. **19**, 25 (January 1987); ibid **20**, 48 (May 1988)
15.127 A. Katzir; Optical fibers in medicine. Sci. Am. **260**, 86 (May 1989)

15.128 H. Schmidt-Kloiber, E. Reichel: Laser lithotripsie, in [Ref.15.118, VI, Sect.2.12.1]
15.129 R. Steiner (ed.): *Laser Lithotripsy* (Springer, Berlin, Heidelberg 1988)
R. Pratesi, C.A. Sacchi (eds.): *Lasers in Photomedicine and Photobiology*, Springer Ser. Opt. Sci., Vol.31 (Springer, Berlin, Heidelberg 1982)
L. Goldmann (ed.): *The Biomedical Laser* (Springer, Berlin, Heidelberg 1981)
15.130 W. Simon, P. Hering: Laser-induzierte Stoßwellenlithotripsie an Nieren- und Gallensteinen. Laser Optoelektron. **19**, 33 (January 1987)
15.131 D. Beaucamp, R. Engelhardt, P. Hering, W. Meyer: Stone identification during laser-induced shockwave lithotripsy, in *Proc. 9th Congress Laser 89*, ed.by W. Waidelich (Springer, Berlin, Heidelberg 1990)
15.132 R. Engelhardt, W. Meyer, S. Thomas, P. Oehlert: Laser-induzierte Schockwellen-Lithotripsie mit Mikrosekunden Laserpulsen. Laser Optoelektr. **20**, 36 (April 1988)
15.133 S.P. Dretler: Techniques of laser lithotripsy. J. Endovrology **2**, 123 (1988)
B.C. Ihler: Laser lithotripsy: system and fragmentation processes closely examined. Laser Optoelektron. **24**, 76 (April 1992)

2. Lecture

Time dependent Spectroscopy

11.2.2 Optical Correlator for Measuring Ultrashort Pulses

For measurements of optical pulse widths below 1 ps the best choice is a correlation technique which is based on the following principle: The optical pulse with the intensity profile $I(t) = c\epsilon_0|E(t)|^2$ and the halfwidth ΔT is split into two pulses $I_1(t)$ and $I_2(t)$, which travel different path lengths s1 and s2 before they are again superimposed (Fig.11.30). For a path difference $\Delta s = s1 - s2$ the pulses are separated by the time interval $\tau = \Delta s/c$ and their coherent superposition yields the total intensity

$$I(t,\tau) = c\epsilon_0[E_1(t) + E_2(t+\tau)]^2 \,. \tag{11.23}$$

A *linear* detector has the output signal $S_L(t) = aI(t)$. If the time constant T of the detector is large compared to the pulse length ΔT, the output signal is

$$S_L(\tau) = a\,\langle I(t,\tau)\rangle = \frac{a}{T}\int_{-T/2}^{+T/2} I(t,\tau)\,dt \,. \tag{11.24}$$

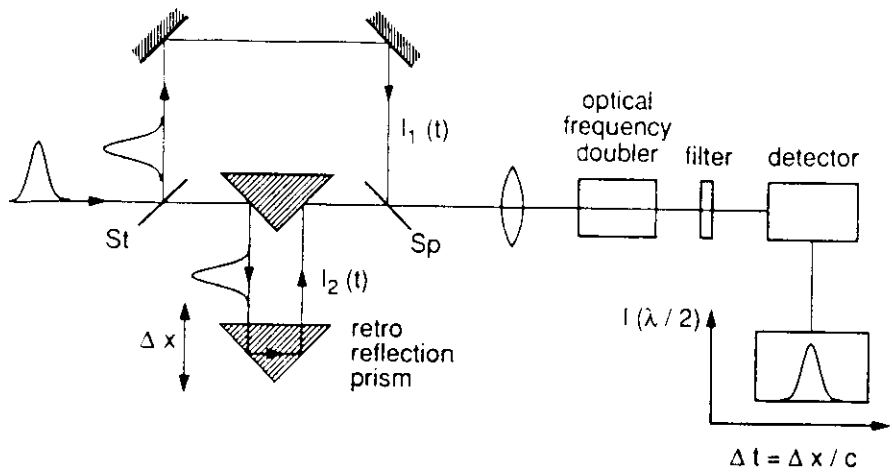

Fig.11.30. Optical correlator with translation-retro-reflecting prism and second-harmonic generation

For equal amplitudes of the two pulses $E_1(t) = E_2(t) = E_0(t)\cos\omega t$ the integrand becomes

$$I(t,\tau) = c\epsilon_0[E_0(t)\cos\omega t + E_0(t+\tau)\cos\omega(t+\tau)]^2 \qquad (11.25)$$

and the integration yields

$$S_L(\tau) = 2c\epsilon_0 a\left\{\langle E_0{}^2\rangle + \frac{1}{T}\int_{-\frac{1}{2}T}^{+\frac{1}{2}T}[E_0(t)\,E_0(t+\tau)\cos\omega t\cos\omega(t+\tau)]\,dt\right\}. \qquad (11.26)$$

For strictly monochromatic CW light ($E_0(t)$ = const) the integral equals $TE_0{}^2\cos\omega\tau$ and the signal

$$S_L(\tau) = 2ac\epsilon_0 E_0{}^2(1+\cos\omega\tau) \qquad (11.27)$$

becomes an oscillatory function of τ with the period $\Delta\tau = \pi/\omega = 1/(2\nu) = \lambda/2c$ (two-beam interference, see Sect.4.2).

Mode-locked pulses of duration ΔT and spectral width $\Delta\omega \approx 2\pi/\Delta T$ are composed of many modes with different frequencies ω. The oscillations of these modes have different periods $\Delta\tau(\omega) = \pi/\omega << T$ and the average over a time interval $T > \Delta T$ yields a value of zero for the integral. *A linear detector with a time constant* $T >> \tau$ *would therefore give an output signal which is independent of* τ *and which yields no information on the time profile* I(t)!. This is obvious, because the detector measures only the integral over $I_1(t)+I_2(t+\tau)$, i.e., the sum of the energies of the two pulses, which is independent of the delay time τ as long as $T > \tau$. *Linear detectors* with the time resolution T can therefore not be used for the measurement of ultrashort pulses with $\Delta T < T$.

If, however, the two pulses are focussed into a nonlinear optical crystal which doubles the optical frequency, the intensity of the 2nd harmonics

$I(2\omega) \propto (I_1+I_2)^2$ is proportional to the *square* of the incident intensity (Sect.5.7) and the measured averaged signal $S(2\omega,\tau) \propto I(2\omega,\tau)$ becomes

$$\langle S_{NL}(2\omega,\tau)\rangle = \frac{a}{T}\int_{-T/2}^{+T/2} I(2\omega,t,\tau)\,dt$$

$$= a[\langle I_1^2\rangle + \langle I_2^2\rangle + 2\langle I_1(t)\,I_2(t+\tau)\rangle]\,. \qquad (11.28)$$

The first two terms are independent of τ and give a constant background. However, the third term depends on the delay time τ and contains the wanted information on the pulse profile I(t). The detector signal $S(2\omega,\tau)$ measured versus the delay time τ, therefore gives the wanted information on the time profile of $I(\omega,t)$.

Note the difference between linear detection (11.25) and nonlinear detection (11.28). With linear detection the *sum* $I_1(t)+I_2(t+\tau)$ is measured which is independent of τ as long as $\tau < T$. The nonlinear detector measures the signal $S(2\omega,\tau)$ that contains the *product* $I_1(t)\,I_2(t+\tau)$ which does depend on τ as long as τ is smaller than the maximum width of the pulses.

The τ-independent background in (11.28) can be suppressed, when the two beams are focussed into the doubling crystal under different angles $\pm\beta/2$ against the z-direction (Fig.11.31) where the signal $S(2\omega)$ is detected. If the phase-matching conditions for the doubling crystal (Sect.5.7) is chosen in such a way that for two photons out of the same beam no phase matching occurs, but only for one photon out of each beam, then the two first terms in (11.28) do not contribute to the signal [11.89,90]. In another method of background-free pulse measurements the polarization plane of one of the two beams in Fig.11.31 is turned in such a way, that a properly oriented doubling crystal (generally a KDP crystal) fulfills the phase-matching condition only if the two photons come each from a different beam [11.91].

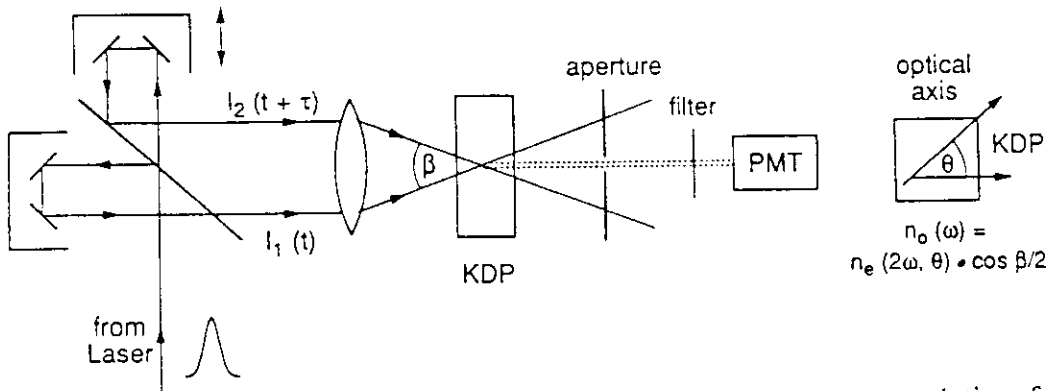

Fig.11.31. Background-free measurement of the second-order correlation function $G^{(2)}(\tau)$ by choosing the phase-matching condition properly. (The spectral filter suppresses scattered light of the fundamental wave at ω. KDP: Kalium-dihydrogen-phosphate crystal for frequency doubling)

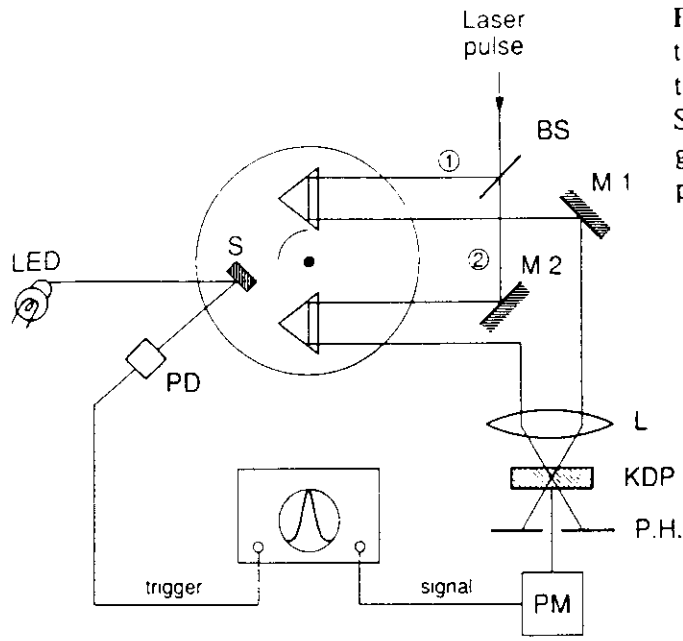

Fig.11.32. Rotating autocorrelator, allowing the direct observation of the correlation signal $S(2\omega,\tau)$ on a scope which is triggered by the output signal of the photodiode PD

In the methods discussed above, one of the retroreflectors is mounted on a translational stage moved via micrometer screws by a step motor while the signal $S(2\omega,\tau)$ is recorded. Since τ must be larger than ΔT, the translational move should be, at least, $\Delta S = \frac{1}{2} c\tau \geq \frac{1}{2} c\Delta T$. For pulses of 10 ps this means $\Delta S \geq 1.5$ mm. With a rotating correlator (Fig.11.32) the signal $S(2\omega,\tau)$ can be directly viewed on a scope, which is very useful when optimizing the pulse width. Two retroreflecting prisms are mounted on a rotating disc. During a certain fraction ΔT_{rot} of the rotation period T_{rot} the reflected beams reach the mirrors M1 and M2 and are focussed into the KDP crystal. The viewing oscilloscope is triggered by a pulse obtained by reflecting the light of a LED onto the photodetector PD.

Instead of using optical frequency-doubling also other nonlinear effects can be used, such as two-photon absorption in liquids or solids, which can be monitored by the emitted fluorescence. If the optical pulse is again split into two pulses travelling in the opposite $\pm z$-directions through the sample cell (Fig.11.33) the spatial intensity profile $I_{FL}(z) \propto I^2(\omega,\tau)$ can be imaged by a magnifying optics onto a videcon or an image intensifier. Since a pulse width $\Delta T = 1$ ps corresponds to a path length of 0.3 mm this technique, based on the spatial resolution of the fluorescence intensity, is limited to pulse widths $\Delta T \geq 0.3$ ps. For shorter pulses the delay time τ between the pulses has to be varied and the total fluorescence

$$I_{FL}(\tau) = \int I(z,\tau)\,dz \tag{11.29}$$

has to be measured as a function of τ [11.92,93].

All these devices, which are called *optical correlators*, measure the correlation between the field amplitude E(t) or the intensity I(t) at the time t and its values $E(t+\tau)$ or $I(t+\tau)$ at a later time. These correlations are math-

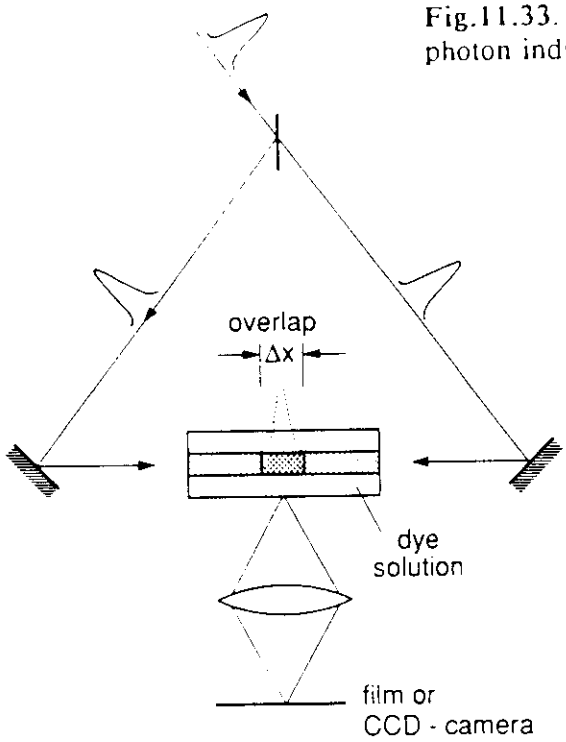

Fig.11.33. Measurement of short pulses via the two-photon induced fluorescence

ematically expressed by normalized correlation functions of order k. The normalized first order correlation function

$$G^{(1)}(\tau) = \frac{\int_{-\infty}^{+\infty} E(t)\cdot E(t+\tau)\,dt}{\int_{-\infty}^{+\infty} E^2(t)\,dt} = \frac{\langle E(t)\cdot E(t+\tau)\rangle}{\langle E^2(t)\rangle} \qquad (11.30)$$

describes the correlation between the field amplitudes at times t and $t+\tau$. From (11.30) we obtain $G^{(1)}(0) = 1$ and for pulses with a finite pulse duration ΔT (11.30) yields $G^{(1)}(\infty) = 0$.

The normalized second-order correlation function

$$G^{(2)}(\tau) = \frac{\int I(t)\cdot I(t+\tau)\,dt}{\int I^2(t)\cdot dt} = \frac{\langle I(t)\cdot I(t+\tau)\rangle}{\langle I^2(t)\rangle} \qquad (11.31)$$

describes the *intensity* correlation, where again $G^{(2)}(0) = 1$. The correlation signal (11.28) after the optical frequency doubler can be written in terms of $G^{(2)}(\tau)$ for $I_1 = I_2 = I/2$ as

$$S_{NL}(2\omega,\tau) = A[G^{(2)}(0) + 2G^{(2)}(\tau)] = A[1 + 2G^{(2)}(\tau)]\,. \qquad (11.32)$$

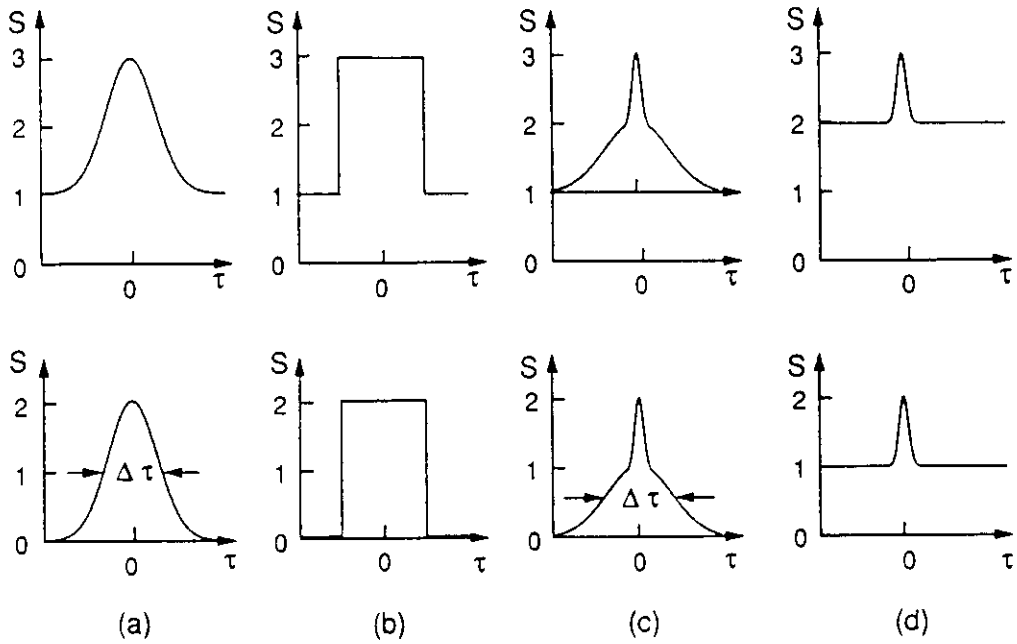

Fig.11.34a-d. Autocorrelation signal $S \propto G^{(2)}(\tau)$ for different pulse profiles without background suppression (*upper part*) and with background suppression (*lower part*): (a) Fourier limited Gaussian pulse, (b) rectangular pulse, (c) single noise pulse, and (d) continuous noise

Without background suppression this yields for completely overlapping pulses $S(2\omega,\tau = 0) = 3A$ and for completely separated pulses $S(2\omega,\tau>>T) = A$.

For methods with background suppression no signal is obtained for $\tau >> T$. It is important to note that the profile $S(\tau)$ of the correlation signal depends on the time profile I(t) of the light pulse. For illustration Fig.11.34a depicts the signal $S(2\omega,\tau)$ of Fourier-limited pulses with the Gaussian profile $I(t) = I_0 \exp(-t^2/0.36\Delta T^2)$ with and without background suppression. From the halfwidth $\Delta\tau$ of the signal the halfwidth ΔT of the pulses can only be derived if the pulse profile I(t) is known. In Table 11.2 the ratio $\Delta\tau/\Delta T$ and the products $\Delta T \cdot \Delta\nu$ are compiled for different pulse profiles I(t) while Fig.11.34a-c illustrates the corresponding profiles and contrasts of $G^{(2)}(\tau)$. Even noise pulses and continuous random noise result in a maximum of the correlation function $G^{(2)}(\tau)$ at $\tau = 0$ ((Fig.11.34d) and the contrast becomes $G^{(2)}(0)/G^{(1)}(\infty) = 2$ [11.89,94]. For the determination of the real pulse profile one has to measure the function $G^{(2)}(\tau)$ over a wider range of delay times τ. Generally a model profile is assumed and the calculated functions $G^{(2)}(\tau)$ and even $G^{(3)}(\tau)$ are compared with the measured ones [11.95].

Table 11.2. Ratios $\Delta\tau/\Delta T$ of the width $\Delta\tau$ of the autocorrelation profile and ΔT of the pulse I(t) and products $\Delta\nu\cdot\Delta T$ of spectral widths and duration ΔT of pulses with different profiles I(t)

Pulse profile	Mathematical expression for I(t)	$\Delta\tau/\Delta T$	$\Delta\nu\cdot\Delta T$
Rectangular	$\begin{cases} I_0 \text{ for } 0 \le t \le \Delta T \\ 0 \text{ elsewhere} \end{cases}$	1	0.886
Gaussian	$I_0 \exp[-t^2/(0.36\Delta T^2)]$	$\sqrt{2}$	0.441
$Sech^2$	$sech^2(t/0.57\Delta T)$	1.55	0.315
Lorentzian	$[1 + (2t/\Delta T)^2]^{-1}$	2	0.221

11.3 Lifetime Measurements with Lasers

Measurements of lifetimes of excited atomic or molecular levels are of great interest for many problems in atomic, molecular, or astrophysics as can be seen from the following three examples:

(i) From the measured lifetimes $\tau_k = 1/A_k$ of levels $|k\rangle$ which may decay by fluorescence into the lower levels $|m\rangle$, the absolute transition probability $A_k = \Sigma_m A_{km}$ can be determined (Sect.2.6). From the measurements of relative intensities I_{km} of transitions $|k\rangle \rightarrow |m\rangle$ the absolute transition probabilities A_{km} can then be obtained. This yields the transition dipole matrix elements $\langle k|\mathbf{r}|m\rangle$ (Sect.2.6.4). The values of these matrix elements are sensitively dependent on the wave functions of upper and lower state. Lifetime measurements therefore represent crucial tests for the quality of computed wave functions and can be used to optimize models of the electron distribution in complex atoms or molecules.

(ii) The intensity decrease $I(\omega, z) = I_0 e^{-\alpha(\omega)z}$ of light passing through absorbing samples depends on the product $\alpha(\omega)z = N_i \sigma_{ik}(\omega)z$ of the absorber density N_i and the absorption cross section σ_{ik}. Since σ_{ik} is proportional to the transition probability A_{ik} (2.22,34) it can be determined from lifetime measurements, see Item (i). Together with measurements of the absorption coefficient $\alpha(\omega)$ the density N_i of the absorbers can be determined. This problem is very important for the test of models for stellar atmospheres [11.96]. A well known example are the measurements of absorption profiles of Fraunhofer lines in the solar spectrum. They yield density and temperature profiles and the abundance of the elements in the sun's atmosphere

(photosphere and chromosphere). The knowledge of transition probabilities allows absolute values of these quantities to be determined.

(iii) Lifetime measurements are not only important to gain information on the dynamics of excited states but also for the determination of absolute cross sections for quenching collisions. The probability R_{kn} per second for the collision-induced transition $|k\rangle \rightarrow |n\rangle$ in an excited atom or molecule A

$$R_{kn} = \int_0^\infty N_B(v)\,\sigma_{kn}(v)\,v\,dv = N_B\,\langle\sigma_{kn}^{coll}\rangle\,\bar{v} \tag{11.34}$$

depends on the density N_B of the collision partners B, the collision cross section σ_{kn}^{coll} and the mean relative velocity $\bar{v}$. The total deactivation probability P_k of an excited level $|k\rangle$ is the sum of radiative probability $A_k = \Sigma_m A_{km} = 1/\tau^{rad}$ and the collisional deactivation probability R_k. Since the effective lifetime is $\tau_k{}^{eff} = 1/P_k$ we obtain the equation

$$\frac{1}{\tau_k{}^{eff}} = \frac{1}{\tau_k{}^{rad}} + \frac{1}{R_k} \quad \text{with} \quad R_k = \sum_n R_{kn}\,. \tag{11.35}$$

In a gas cell at the temperature T the mean relative velocity between collision partners A and B with masses M_A, M_B is

$$\bar{v} = \sqrt{8kT/\pi\mu} \quad \text{with} \quad \mu = \frac{M_A M_B}{M_A + M_B}\,. \tag{11.36}$$

Using the thermodynamic equation of state $p = N \cdot kT$ we can replace the density N_B in (11.34) by the pressure p and obtain the *Stern-Vollmer equation*:

$$\frac{1}{\tau_k{}^{eff}} = \frac{1}{\tau_k{}^{rad}} + b\sigma_k p \quad \text{with} \quad b = (\pi\mu/8kT)^{1/2}\,. \tag{11.37}$$

It represent a straight line when $1/\tau^{eff}$ is plotted versus p (Fig. 11.35). The slope $\tan\alpha = b\sigma_k$ yields the total quenching cross section σ_k and the intersect with the axis p = 0 gives the radiative lifetime $\tau_k{}^{rad} = \tau_k{}^{eff}$ (p=0).

In the following subsections we will discuss some experimental methods of lifetime-measurements [11.97,98]. Nowadays lasers are generally used for the selective population of excited levels. In this case the induced emission, which contributes to the depletion of the excited level, has to be taken into account, if the exciting laser is not switched off during the fluorescence detection. The rate equation for the time-dependent population density of the level $|k\rangle$, which gives the effective lifetime $\tau_k{}^{eff}$, is then

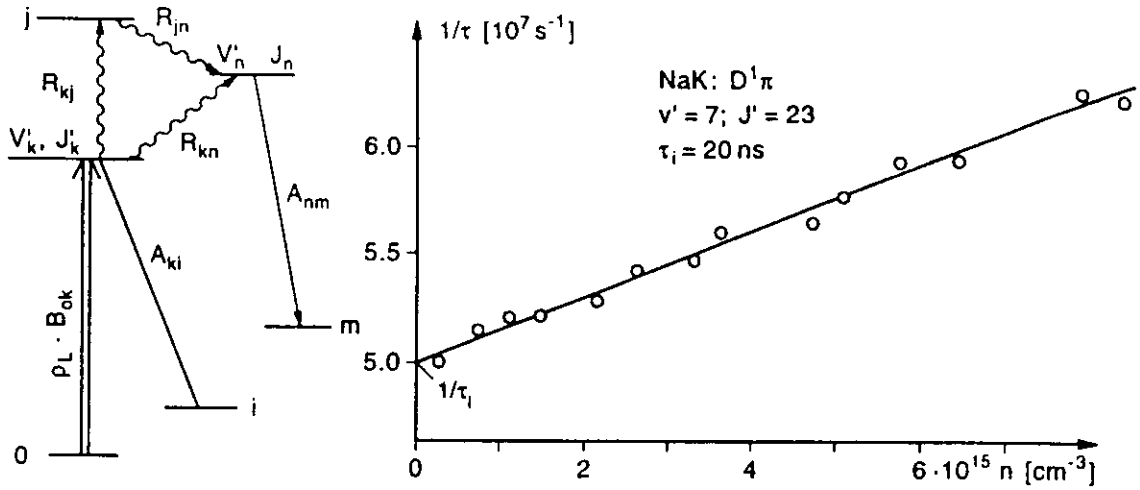

Fig.11.35. Collisional depopulation of the excited level (v'_k, J'_k) of a molecule and example of a Stern-Vollmer plot for the NaK level $D^1\Pi_u(v'=7, J'=13)$

$$\frac{dN_k}{dt} = + N_i B_{ik} \rho_L - N_k(A_k + R_k + B_{ki} \rho_L) \tag{11.38}$$

where ρ_L is the spectral energy density of the exciting laser which is tuned to the transition $|i\rangle \rightarrow |k\rangle$. The solution $N_K(t) \propto I_{Fl}(t)$ of (11.38) depends on the time profile $I_L(t) = c\rho_L(t)$ of the excitation laser.

11.3.1 Phase-Shift Method

If the laser is tuned to the center ω_{ik} of an absorbing transition $|i\rangle \rightarrow |k\rangle$ the detected fluorescence intensity I_{FL} monitored on the transition $|k\rangle \rightarrow |m\rangle$ is proportional to the laser intensity I_L as long as saturation can be neglected. In the *phase-shift method* the laser intensity is modulated at the frequency $f = \Omega/2\pi$ (Fig.11.36a) according to

$$I_L(t) = \frac{1}{2} I_0(1 + a\sin\Omega t)\cos^2\omega_{ik} t \,. \tag{11.39}$$

Inserting (11.39) with $I_L(t) = c\rho_L(t)$ into (11.38) yields the time-dependent population density $N_k(t)$ of the upper level, and therefore also the fluorescence power $P_{FL}(t) = N_k(t) A_{km}$ emitted on the transition $|k\rangle \rightarrow |m\rangle$. The result is

$$P_{FL}(t) = b\left[1 + \frac{a\sin(\Omega t + \Phi)}{[1 + (\Omega\tau_{eff})^2]^{1/2}}\right]\cos^2\omega_{km} t \tag{11.40}$$

where the constant $b \propto N_0 \sigma_{0k} I_L V$ depends on the density N_0 of the absorbing molecules, the absorption cross section σ_{0k}, the laser intensity I_L, and the excitation volume V seen by the fluorescence detector. Since the

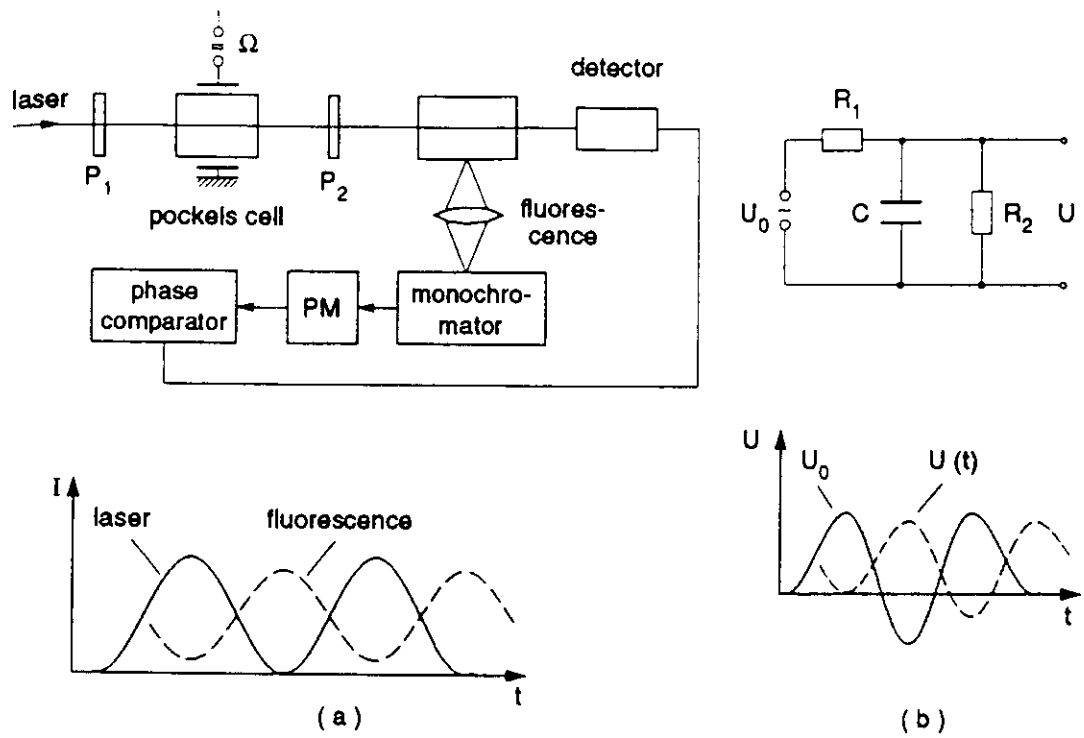

Fig.11.36a,b. Phase-shift method for the measurement of excited-state lifetimes: (a) experimental arrangement and (b) equivalent electric network

detector averages over the optical oscillations ω_{km} we obtain $\langle\cos^2\omega_{km}\rangle = 1/2$ and (11.40) gives similar to (11.39) a sinewave-modulated function with the phase shift ϕ against the exciting intensity $I_L(t)$. This plase shift depends on the modulation frequency Ω and the effective lifetime τ_{eff}. The evaluation yields

$$\tan\phi = \Omega\tau_{eff} \ . \qquad (11.41)$$

According to (11.35-38) the effective lifetime is determined by the inverse sum of all deactivation processes of the excited level $|k\rangle$. In order to obtain the spontaneous lifetime $\tau_{spont} = 1/A_k$ one has to measure $\tau_{eff}(p, I_L)$ at different pressures p and different laser intensities I_L, and extrapolate the results towards $p \to 0$ and $I_L \to 0$.

The influence of induced emission is a definite drawback of the phase-shift method.

Note: This problem of exciting atoms with sinewave-modulated light and determining the mean lifetime of their exponential decay from measurements of the phase shift ϕ is mathematically completely equivalent to the well-known problem of charging a capacitor C from an AC source with the voltage $U_0(t) = U_1\sin\Omega t$ through the resistor R_1 with simultaneous discharging through a resistor R_2 (Fig.11.36b). The equation corresponding to (11.38) is here

$$C\frac{dU}{dt} = \frac{U_0 - U}{R_1} - \frac{U}{R_2} \tag{11.42}$$

which has the solution

$$U = U_2 \sin(\Omega t - \phi) \quad \text{with} \quad \tan\phi = \Omega \frac{R_1 R_2 C}{R_1 + R_2} \tag{11.43}$$

where

$$U_2 = U_0 \frac{R_2}{[(R_1+R_2)^2 + (\Omega C R_1 R_2)^2]^{1/2}} .$$

A comparison with (11.40) shows that the mean lifetime τ corresponds to the time constant $\tau = RC$ with $R = R_1R_2/(R_1+R_2)$ and the laser intensity to the charging current $I(t) = (U_0-U)/R_1$.

Equation (11.41) anticipates a pure exponential decay. This is justified if a single upper level $|k\rangle$ is selectively populated. If several levels are simultaneously excited the fluorescence power $P_{FL}(t)$ represents a superposition of decay functions with different decay times τ_k. In such cases the phase shifts $\phi(\Omega)$ and the amplitudes $a/(1+\Omega^2\tau^2)^{1/2}$ have to be measured for different modulation frequencies Ω. The mathematical analysis of the results allows one to separate the contributions of the simultaneously excited levels to the decay curve and to determine the different lifetimes of these levels [11.99]. A better solution is, however, if the fluorescence is dispersed by a monochromator and the detector monitors selectively the transitions from the different excited levels $|k_n\rangle$ separately.

11.3.2 Single-Pulse Excitation

The molecules are excited by a short laser pulse. The trailing edge of this pulse should be short compared with the decay time of the excited level, which is directly monitored after the end of the excitation pulse. Either the time-resolved LIF on transitions $|k\rangle \rightarrow |m\rangle$ to lower levels $|m\rangle$ is detected or the time-dependent absorption of a second laser, which is tuned to the transition $|k\rangle \rightarrow |j\rangle$ to higher levels $|j\rangle$.

The time-dependent fluorescence can be viewed either with an oscilloscope or may be recorded by a transient recorder. Another possibility is based on a boxcar integrator, which transmits the signal through a gate that opens only during a selected time interval Δt (Sect.4.5.5). After each successive excitation pulse the delay ΔT of the gate is increased by T/m. After m excitation cycles the whole time window T has been covered (Fig. 11.37). The direct observation of the decay curve on an oscilloscope has the advantage that nonexponential decays can be recognized immediately. For sufficiently intense fluorescence one needs only a single excitation pulse, although generally averaging over many excitation cycles will improve the signal-to noise ratio.

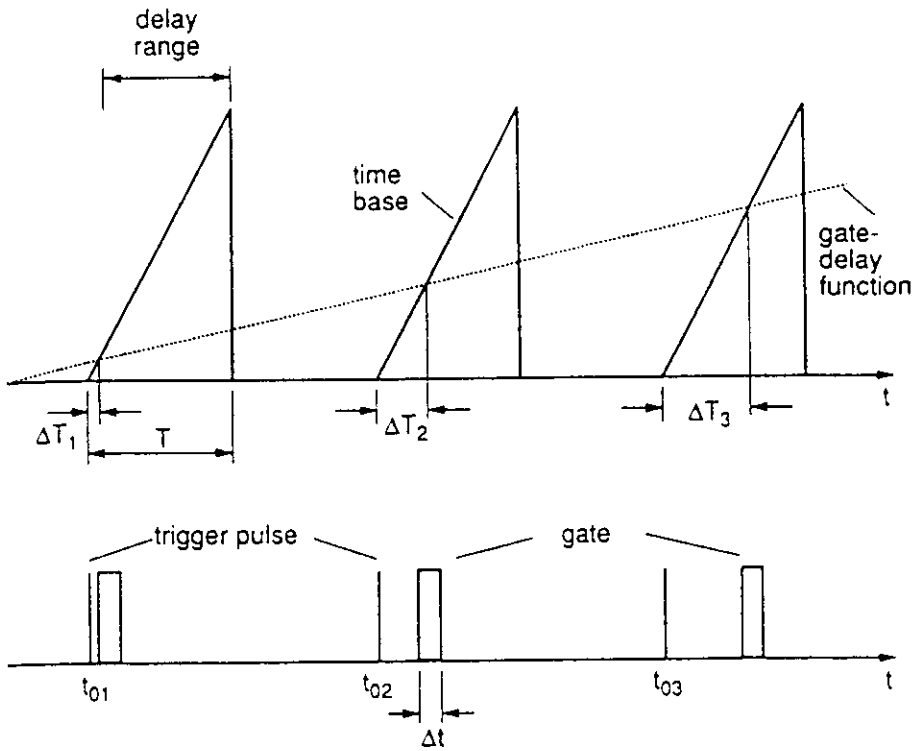

Fig.11.37. Lifetime measurements with a gated boxcar system with successively increasing gate delay time

This technique of single-pulse excitation is useful for low repetition rates. Examples are the excitation with pulsed dye lasers pumped by Nd:YAG or excimer lasers [11.97, 100].

11.3.3 Delayed-Coincidence Technique

As in the previous method the delayed-coincidence technique also uses short laser pulses for the excitation of selected levels. However, here the pulse energy is kept so low, that the detection probability P_D of a fluorescence photon per laser excitation pulse remains small ($P_D \leq 0.1$). If $P_D(t)\,dt$ is the probability of detecting a fluorescence photon in the time interval t to t+dt after the excitation then the mean number $n_{Fl}(t)$ of fluorescence photons detected within this time interval for N excitation cycles ($N >> 1$) is

$$n_{Fl}(t)\,dt = N P_D(t)\,dt\,. \qquad (11.44)$$

The experimental realization is shown schematically in Fig.11.38. Part of the laser pulse is sent to a fast photodiode. The output pulse of this diode at $t = t_0$ starts a Time-Amplitude Converter (TAC) which generates a fast rising voltage ramp $U(t) = (t-t_0)U_0$. A photomulitplier with a large amplification factor generates for each detected fluorescence photon an output pulse that triggers a fast discriminator. The normalized output pulse of the discriminator stops the TAC at time t. The amplitude U(t) of the TAC

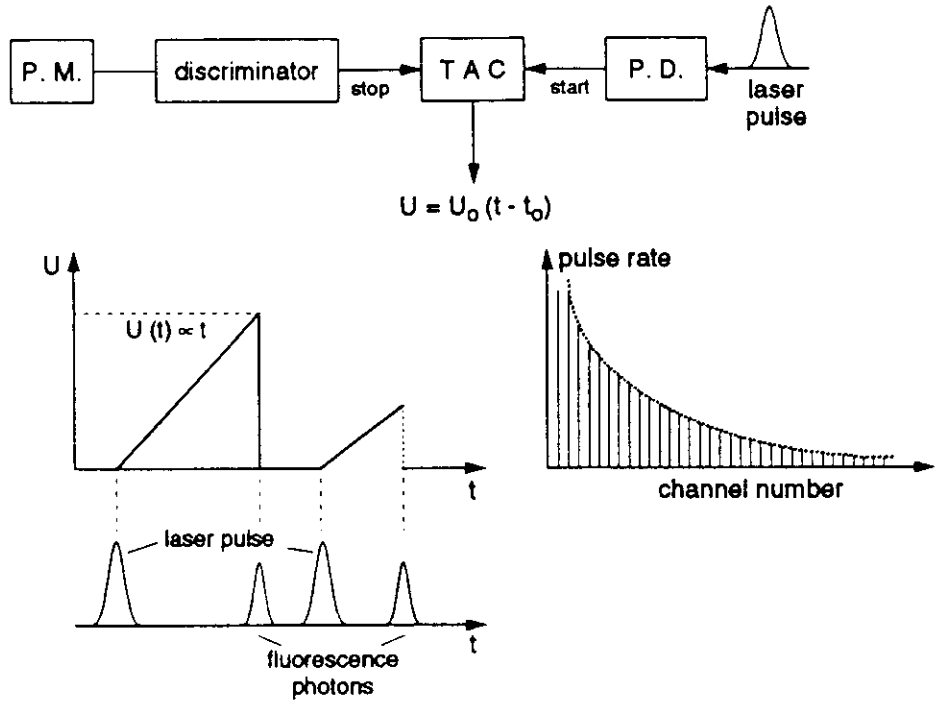

Fig.11.38. Basic principle of lifetime measurements with the delayed coincidence single photon counting technique

output pulse is proportional to the delay time $t-t_0$ between excitation pulse and fluorescence photon emission. These pulses are stored in a multichannel analyzer. The number of events per channel gives the number of fluorescence photons emitted at the corresponding delay time.

The repetition rate f of the excitation pulses is chosen as high as possible since the measuring time for a given signal-to-noise-ratio is proportional to 1/f. An upper limit for f is determined by the fact that the time T between two successive laser pulses should be at least three times the lifetime τ_k of the measured level $|k\rangle$. This technique is therefore ideally suited for excitation with mode-locked or cavity-dumped lasers. There is, however, an electronic bottleneck: The input-pulse rate of a TAC is limited by its dead time τ_D and should be smaller than $1/\tau_D$. It is therefore advantageous to invert the functions of the start-and-stop pulses. The fluorescence pulses (which have a much smaller rate than the excitation pulses) now act as start pulses and the next laser pulse stops the TAC. This means that the time (T-t) is measured instead of T. Since the time T between successive pulses of a mode-locked laser is very stable and can be accurately determined from the mode-locking frequency f = 1/T the time interval between successive pulses can be used for time calibration of the detection system [11.30]. In Fig.11.39 the whole detection system is shown together with a decay curve of an excited level of the Na_2 molecule, measured over a period of 10 min.

More information about the delayed-coincidence method can be found in [11.101].

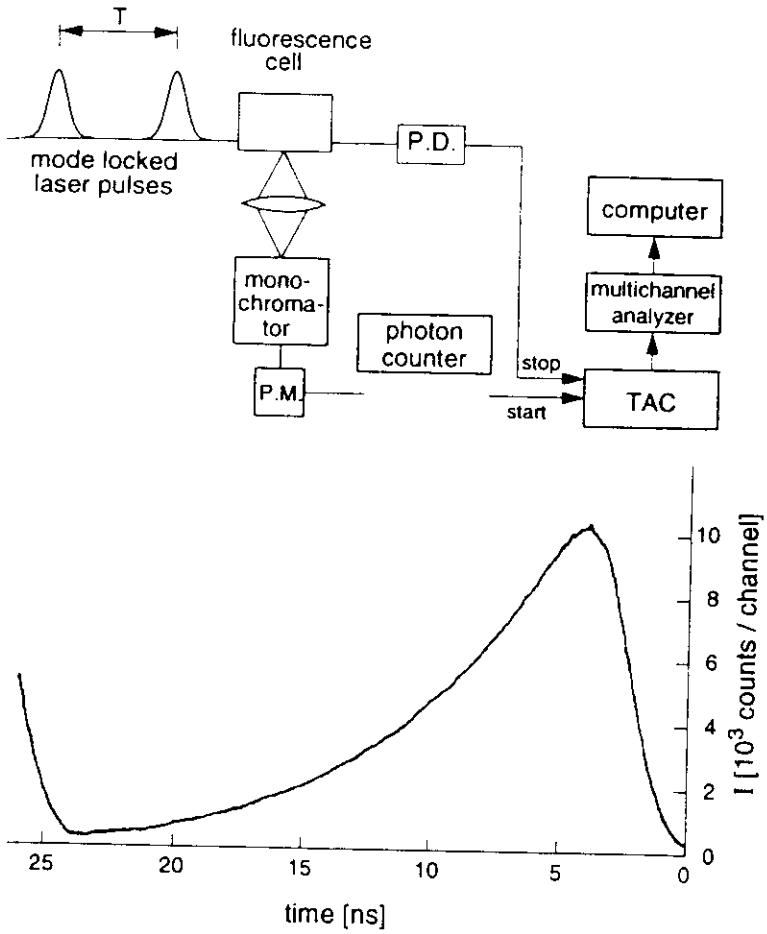

Fig.11.39. Experimental arrangement for lifetime measurements with the delayed coincidence single-photon counting technique and decay curve of the Na_2 ($B^1\Pi_u$ $v'=6$, $J'=27$) level [11.29]

11.3.4 Lifetime Measurements in Fast Beams

The most accurate method for lifetime measurements in the range of $10^{-7} \div 10^{-9}$ s is based on a modern version of an old technique which had been used by N. Wien already 70 years ago [11.102]. Here a time measurement is reduced to a pathlength- and a velocity measurement:

The atomic or molecular ions produced in an ion source are accelerated by the voltage U and focussed to form an ion beam. The different masses are separated by a magnet (Fig.11.40) and the wanted ions are excited at the position x = 0 by a CW-laser beam. The LIF is monitored as a function of the variable distance x between the excitation region and the position of a special photon detector mounted on a precision translational drive. Since the velocity $v = (2eU/m)^{1/2}$ is known from the measured acceleration voltage U the time $t = x/v$ is determined from the measured positions x.

The excitation intensity can be increased if the excitation region is placed inside the resonator of a CW dye laser that is tuned to the selected transition. Before they reach the laser beam, the ions can be preexcited into highly excited long-living levels by gas collisions in a gas cell being dif-

11.4 Pump and Probe Technique

For measurements of very fast relaxation processes with a demanded time resolution below 10^{-10} s most detectors (except the streak camera) are not fast enough. Here the pump and probe technique is the best choice. It is based on the following principle (Fig.11.43).

The molecules under investigation are excited by a fast laser pulse on the transition $|0\rangle \rightarrow |1\rangle$. A probe pulse with a variable time delay τ against the pump pulse probes the time evolution of the population density $N_1(t)$. The time resolution is only limited by the pulse width ΔT of the two pulses but not by the time constants of the detectors!

In early experiments of this kind a fixed-frequency mode-locked Nd-Glass or Nd:YAG laser was used. Both pulses came from the same laser and fortuitious coincidences of molecular transitions with the laser wavelength

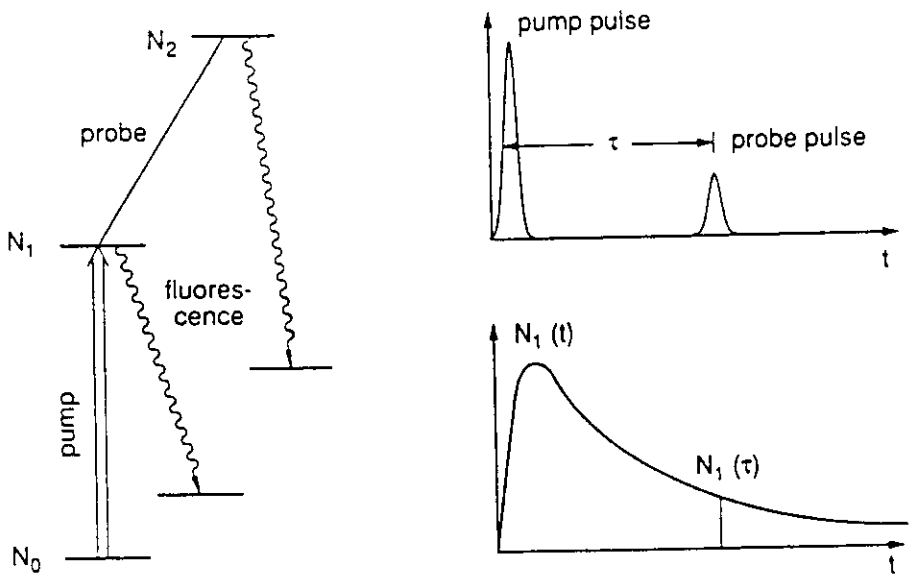

Fig.11.43. Pump-and-probe technique

were utilized [11.108]. The time delay of the probe pulse is realized, as shown in Fig.11.30, by beam splitting and a variable path-length difference. Since the pump and probe pulses coincide with the same transition $|i\rangle \rightarrow |k\rangle$ the absorption of the probe pulse measured as a function of the delay time τ, in fact, monitors the time evolution of the population difference $[N_k(t)-N_i(t)]$. A larger variety of molecular transitions becomes accessible, if the Nd:YAG laser wavelength is Raman shifted (Sect.5.9) into spectral regions of interest [11.109].

A broader application range is opened by a system of two independently tunable mode-locked dye lasers which have to be pumped by the same pump laser in order to synchronize the pump and probe pulses [11.110]. For studies of vibrational levels in the electronic ground states of molecules the difference frequency generation of these two dye lasers can be used as a tunable infrared source for direct excitation of selected levels on infrared-active transitions. Raman active vibrations can be excited by spontaneous or stimulated Raman transitions (Chapt.8).

11.4.4 Real-Time Observations of Molecular Vibrations

The time scale of molecular vibrations is of the order of $10^{-14} \div 10^{-15}$ s. The vibrational frequency of the H_2 molecule, for example, is $\nu_{vib} = 1.3 \cdot 10^{14}$ $s^{-1} \rightarrow T_{vib} = 7.6 \cdot 10^{-15}$ s that of the Na_2 molecule is $\nu_{vib} = 4.5 \cdot 10^{12}$ $s^{-1} \rightarrow$ $T_{vib} = 2 \cdot 10^{-13}$ s and even the heavy I_2 molecule still has $T_{vib} = 5 \cdot 10^{-13}$ s. With conventional techniques one always measures a time average over many vibrational periods.

With femtosecond pump-probe experiments "fast motion pictures" of a vibrating molecule may be obtained and the time behaviour of the wave packets of coherently excited and superimposed molecular vibrations can be mapped. This will be illustrated by the following examples dealing with the dynamics of molecular multiphoton ionisation and fragmentation of Na_2, and its dependence on the phase of the vibrational wave packet in the in-

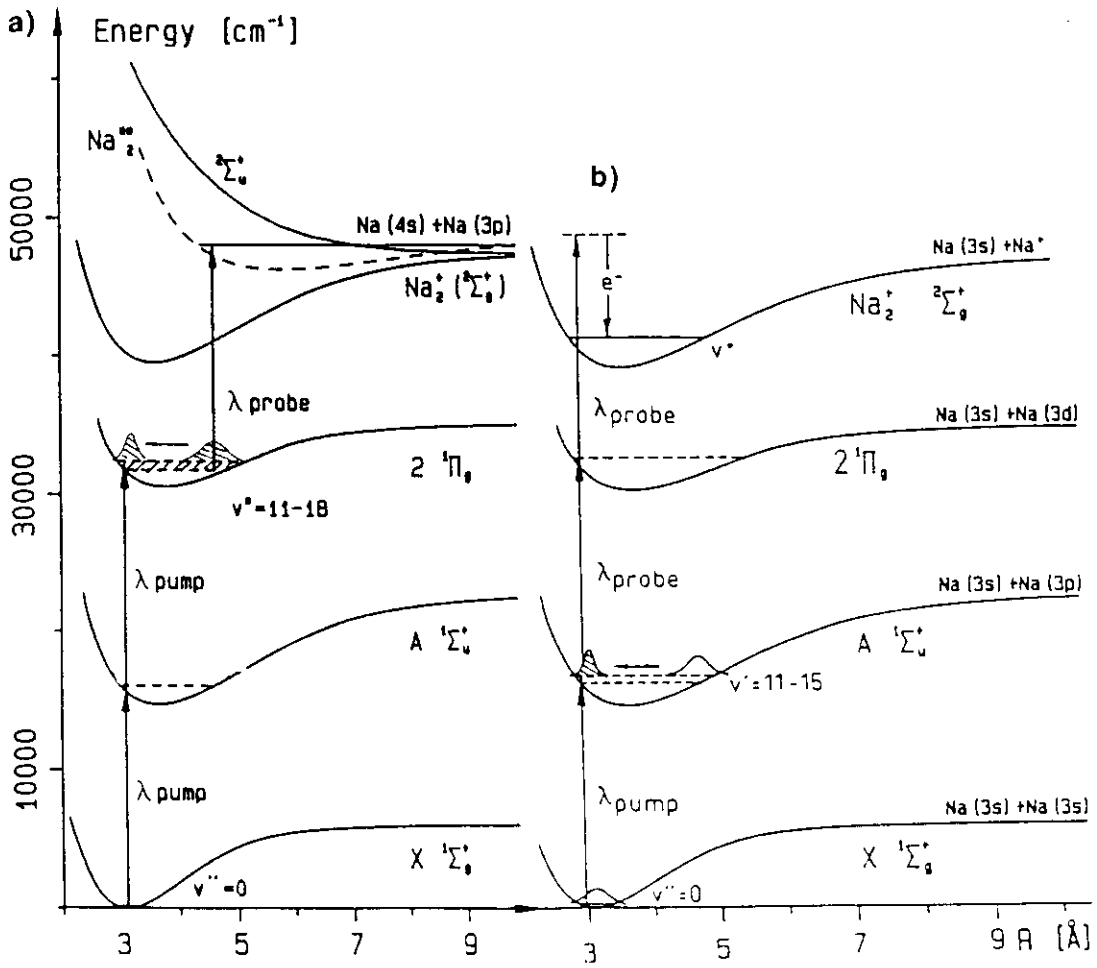

Fig.11.46a,b. Femtosecond spectroscopy of Na_2. (a) Potential curve diagram illustrating the preparation of a vibrational wave packet in the $2^1\Pi_g$ state of Na_2 due to coherent simultaneous two-photon excitation of vibrational levels ($v' = 11 \div 18$). Further excitation by a third photon results in production of $Na_2^{**} \rightarrow Na^+ + Na^*$ from the outer turning point of the wave packet. (b) One-photon excitation of a vibrational wave packet in the $A^1\Sigma_u$ state with subsequent two-photon ionization from the *inner* turning point [11.119]

termediate state [11.118]. There are two pathways for photoionization of cold Na_2 molecules in a supersonic beam (Fig.11.46):

(i) One-photon absorption of a femtosecond pulse (λ = 672nm, ΔT = 70fs, I = 50GW/cm^2) leads to a simultaneous coherent excitation of vibrational levels v′ = 10-14 in the A $^1\Sigma_u$ stae of Na_2 at the inner part of the potential $V_1(R)$. This generates a vibrational wave packet which oscillates at a frequency of 3.10^{12} s^{-1} back and forth between the inner and outer turning point. Resonant enhanced two-photon ionization of the excited molecules by the probe pulse has a larger probability at the inner turning point than at the outer turning point, due to favorable Franck-Condon factors for transitions from the A $^1\Sigma_u$ state to the near resonant intermediate state $2^1\Pi_g$ which enhances ionizing two-photon transitions at small values of the internuclear distance R. The ionization rate $N(Na_2^+, \Delta t)$ monitored as a function of the delay time Δt between the weak pump pulse and the stronger probe

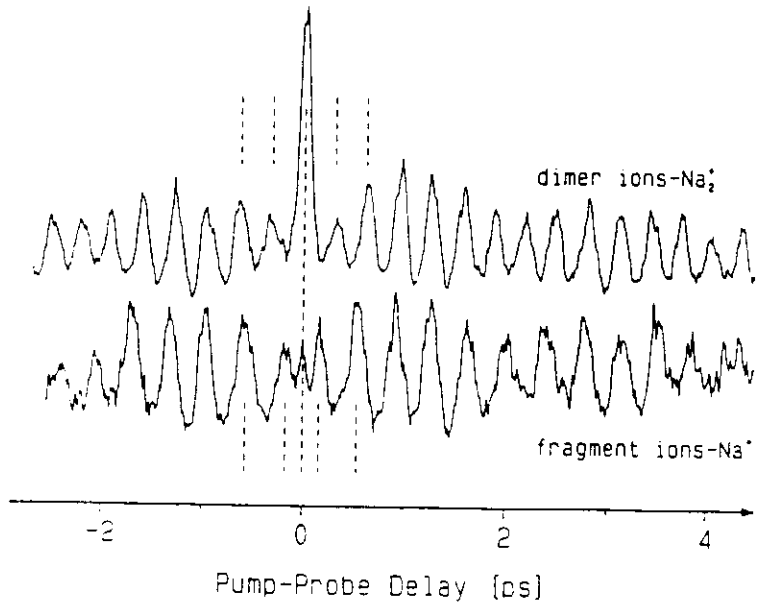

Fig.11.47. Observed ion rates $N(Na_2^+)$ (*upper trace*) and $N(N_a^+)$ as a function of the delay time Δt between the pump and probe pulses [11.119]

pulse yields the upper oscillatory function of Fig.11.47 with a period that matches the vibrational wave-packet period in the $A^1\Sigma_u$ state.

(ii) The second possible competing process is the two-photon excitation of wavepackets of the v′ = 11÷18 vibrational levels in the $2^1\Pi_g$ state of Na_2 by the pump pulse with subsequent one-photon excitation into a doubly excited state of Na_2^{**}, which autoionizes according to

$$Na_2^{**} \rightarrow Na_2^+ + e^- \rightarrow Na^+ + Na^* + e^- ,$$

and results in the generation of Na^+ ions. The number $N(Na^+, \Delta t)$ of atomic ions Na^+, measured as a function of the delay time Δt between pump and probe pulses shows again an oscillatory structure (Fig.11.47, lower trace), but with a time shift of half a vibrational period against the upper trace. In this case the ionization starts from the *outer* turning point of the $2^1\Pi_g$ levels and the oscillatory structure shows a 180° shift and slightly different oscillation period which corresponds to the vibrational period in the $2^1\Pi_g$ state.

The photoelectrons and ions, and their kinetic energies can be measured with two time-of-flight mass spectrometers arranged into opposite directions perpendicular to the molecular and the laser beam [11.120].

3. Lecture

Numerous books have meanwhile been published on laser applications in medical research in hospital practice [15.115-118]. Most of these applications rely on the high laser-output power which can be focussed into a small volume. The strong dependence of the absorption coefficient of living tissue on the wavelength allows selection of the penetration depth of the laser beam by choosing the proper laser wavelength [15.117]. For example, skin carcinoma or portwine marks should be treated at wavelengths for a small penetration depth in order to protect the deeper layers of the epidermia from being damaged, while cutting of bones with lasers or treatment of subcutan cancer must be performed at wavelengths with greater penetration depth. The most spectacular outcomes of laser applications in medicine have been achieved in laser surgery, dermatology, opthalmology and dentistry.

There are, however, also very promising direct applications of laser *spectroscopy* for the solution of problems in medicine. They are based on new diagnostic techniques. Some of them are discussed in this section.

15.5.1 Applications of Raman Spectroscopy in Medicine

During the operation of a patient, the optimum concentration and composition of narcotic gases can be indicated by the composition of the respiratory gases, i.e. with the concentration ratio of $N_2:O_2:CO_2$. This ratio can be measured in vivo with Raman spectroscopy [15.119]. The gas flows through a cell which is placed inside a multipass arrangement for an argon-laser beam (Fig.15.21). In a plane perpendicular to the beam axis several detec-

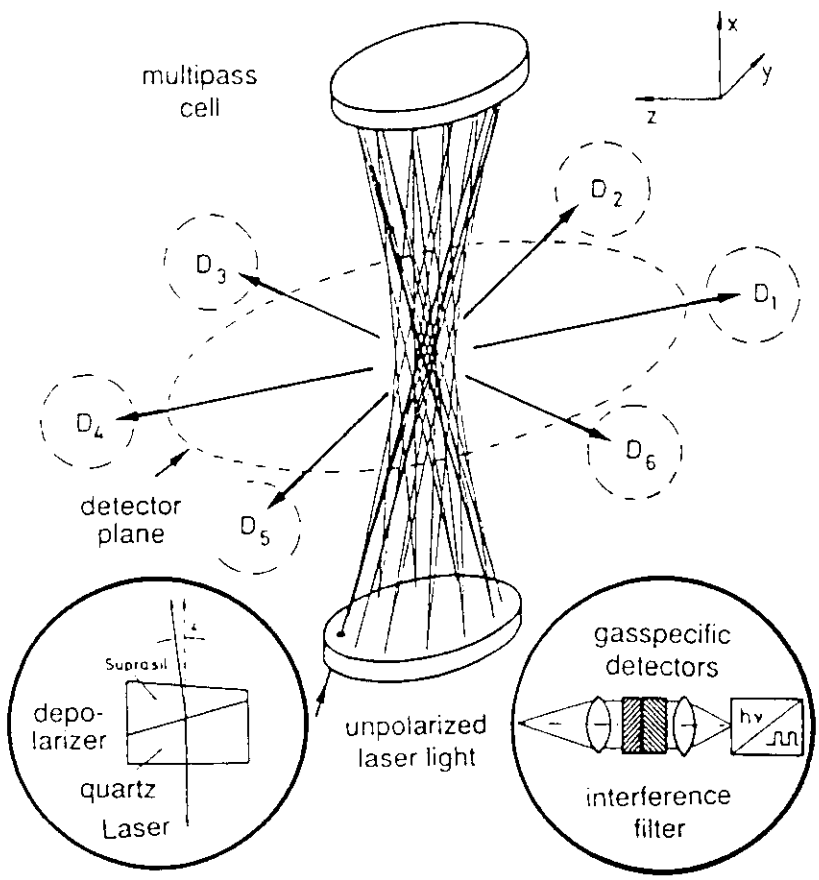

Fig.15.21. Multipass cell and spectrally selective detector arrangement for sensitive Raman spectroscopy and diagnostics of molecular gases [15.119]

tors with special spectral filters are arranged. Each detector monitors a selected Raman line which allows the simultaneous detection of all molecular components of the gas.

The sensitivity of the method is illustrated by Fig.15.22, which depicts the time variation of the CO_2, O_2 and N_2 concentration in the exhaled air of a human patient. Note the variation of the concentrations with changing breathing period. The technique can be used routinely in clinical practice for anesthetic control during operations and obviously also for alcohol tests of car drivers.

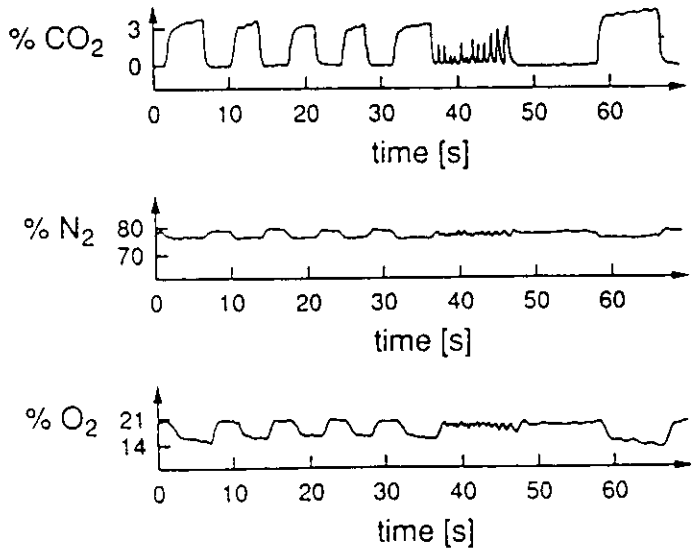

Fig.15.22. CO_2, N_2 and O_2 concentrations of respiratory gases for varying breath periods, measured in vivo with the arrangement of Fig.15.22 [15.119]

15.5.2 Heterodyne Measurements of Ear Drums

A large fraction of ear diseases of elderly people is due to changes in the frequency response of the ear drum. While up to now investigations of such changes had to rely on the subjective response of the patient, novel laser-spectroscopy techniques allow objective studies of frequency-dependent vibrational amplitudes of the ear drum and their local variation for different locations on the drum with a laser Doppler vibrometer (Fig. 15.23). The experimental arrangement is illustrated in Fig.15.24. The output of a diode laser is fed through an optical fiber to the ear drum. The light reflected by the drum is collected by a lens at the end of the fiber and is sent back through the fiber where it is superimposed on a photodetector behind a beam splitter with part of the direct laser light. The ear is exposed to the sound waves of a loudspeaker with variable audio frequency f. The frequency ω of the light reflected by the vibrating ear drum is Doppler shifted. From the frequency spectrum of the heterodyne signals the amplitude A(f) of the illuminated area of the vibrating drum can be derived (Sect.12.6). In order to transfer the heterodyne spectrum in a region with less noise, the laser light is modulated at the frequency $\Omega \approx 40$ MHz by an opto-acoustic modulator producing sidebands at $\omega \pm \Omega$ [15.120].

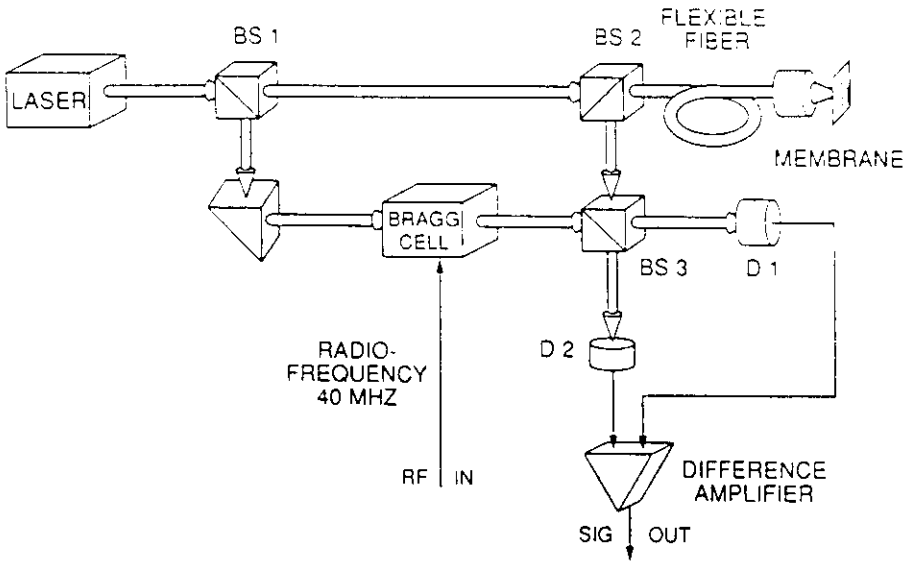

Fig.15.23. Principle of laser Doppler vibrometer

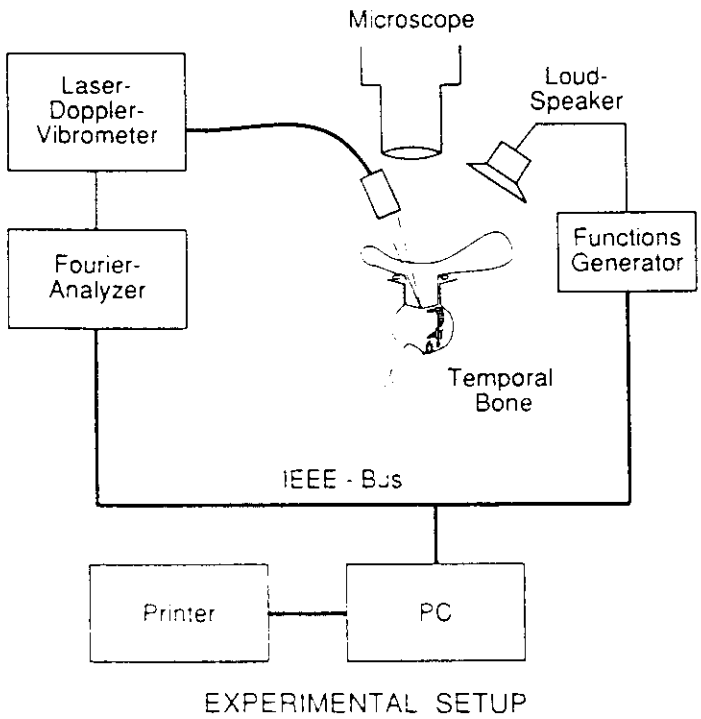

Fig.15.24. Heterodyne measurements of frequency-dependent vibrations of the ear drum and their local variations

15.5.3 Cancer Diagnostics and Therapy with the HPD Technique

Recently, a method for diagnostics and treatment of cancer has been developed which is based on photoexcitation of the fluorescing substance HematoPorphyrin Derivate (HPD) [15.121]. A solution of this substance is injected into the veins and is distributed in the whole body after a few hours. While HPD is released by normal cells after 2÷4 days it is kept by cancer cells for a longer time [15.122]. If a tissue containing HPD is irradiated by a UV laser, it emits a characteristic fluorescence spectrum which can be used for a diagnostic of cancer cells. Figure 15.25 shows the emission spectrum of a tissue with and without HPD, and also the fluorescence of pure HPD in a liquid solution excited by a nitrogen laser at $\lambda = 337$ nm. The experimental arrangement for detecting a cancerous tissue in rats is exhibited in

Fig.15.26 [15.123]. The fluorescence is spectrally resolved by a grating and spatially separated by three slightly folded mirrors which image a cancer region and a region of normal cells onto different parts of the diode array of an optical multichannel analyser (Sect.4.5). A computer subtracts the fluorescence of the normal tissue from that of a cancerous tissue.

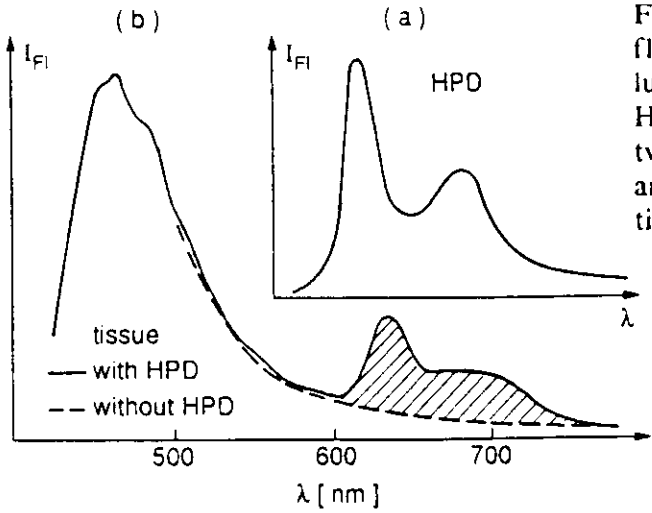

Fig.15.25. Nitrogen-laser-excited fluorescence spectrum of HPD in solution (a) and of tissue (b) without HPD (*dashed curve*), and with HPD two days after injection. The hatched area represents the additional absorption of HPD [15.123]

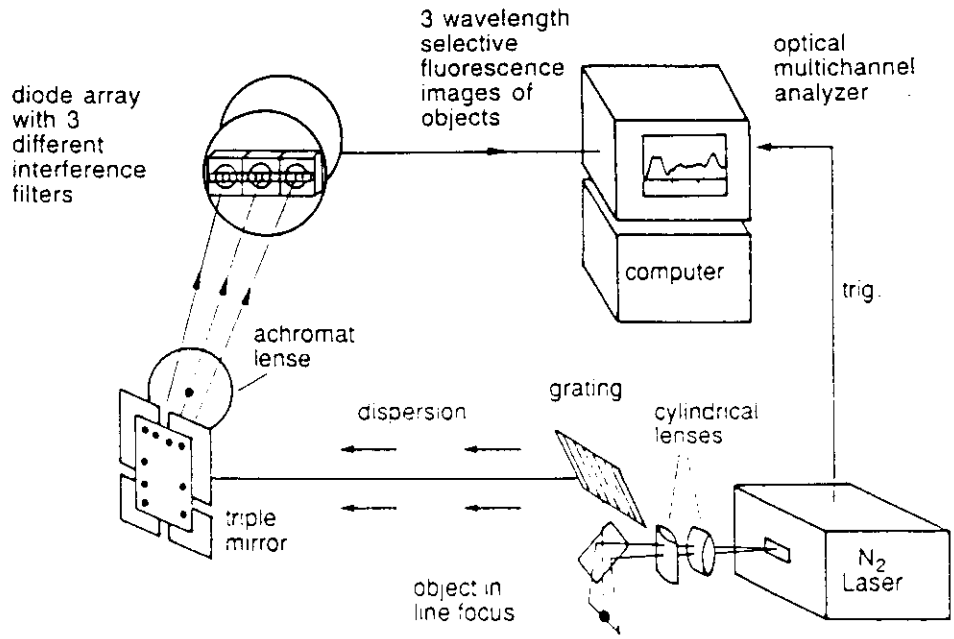

Fig.15.26. Experimental arrangement for cancer diagnostics of rat tissue [15.123]

Absorption of photons in the range 620÷640 nm brings HPD into an excited state, which reacts with normal oxygen in the $O_2(^3\Pi)$ state and transfer it into the $O_2(^1\Delta)$ state which apparently reacts with the surrounding cells and destroys them. Although the exact mechanism of these processes is not yet completely understood, it seems that this HPD method allows a rather selective destruction of cancer cells without too much damage to the normal cells. The technique was developed in the USA, intensively applied in Japan [15.124] and has meanwhile been applied successfully to patients with oesophagus cancer, cervix carcinoma and other kinds of tumors which can be reached by optical fibers without invasive surgery

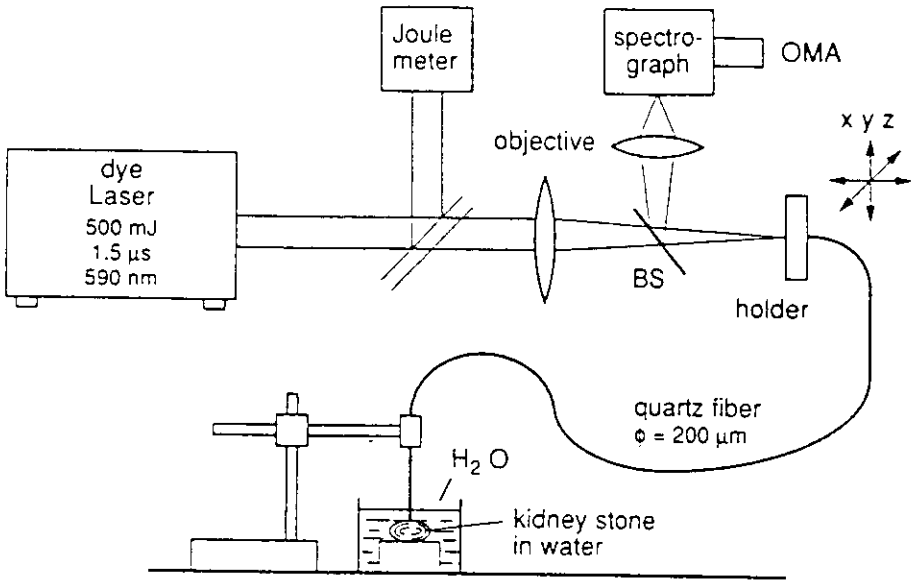

Fig.15.27. Experimental arrangement for the spectral analysis of kidney stones for the determination of stone composition

15.5.4 Laser Lithotripsy

Due to the development of thin, flexible optical fibers with a high damage threshold for the laser radiation [15.126, 127], inner organs of the human body, such as stomach, bladder, gall or kidneys, can be selectively irradiated by laser radiation. A new technique of breaking gall stones to pieces by irradiation with pulsed lasers (laser lithotripsy) has found increasing interest because it has several advantages compared to the ultrasonic shock-wave lithotripsy [15.128, 129].

The optical fiber of fused quartz is inserted through the urinary channel until it nearly touches the stone that is to be broken. This can be monitored by X-Ray diagnosis or by endoscopy through a fiber bundle which contains, besides the fiber for guiding the laser beam, other fibers for illumination, viewing and monitoring the laser-induced fluorescence.

If the pulse of a flashlamp-pumped dye laser is transported through the fiber and focussed onto the gall stone, the rapid evaporation of the stone material results in a shock wave in the surrounding liquid which leads to a destruction of the stone after several laser shots [15.129]. The necessary laser power and the optimum wavelength depend on the chemical composition of the stone, which generally varies for different patients. It is therefore advantageous to know the stone composition before the distruction in order to choose optimum laser conditions. This information can be obtained by collecting the fluorescence of the evaporated stone material at low laser powers through an optical fiber (Fig. 15.27). The fluorescence spectrum is monitored with an optical multichannel analyser and a computer gives, within seconds, the wanted information about the stone composition [15. 130].

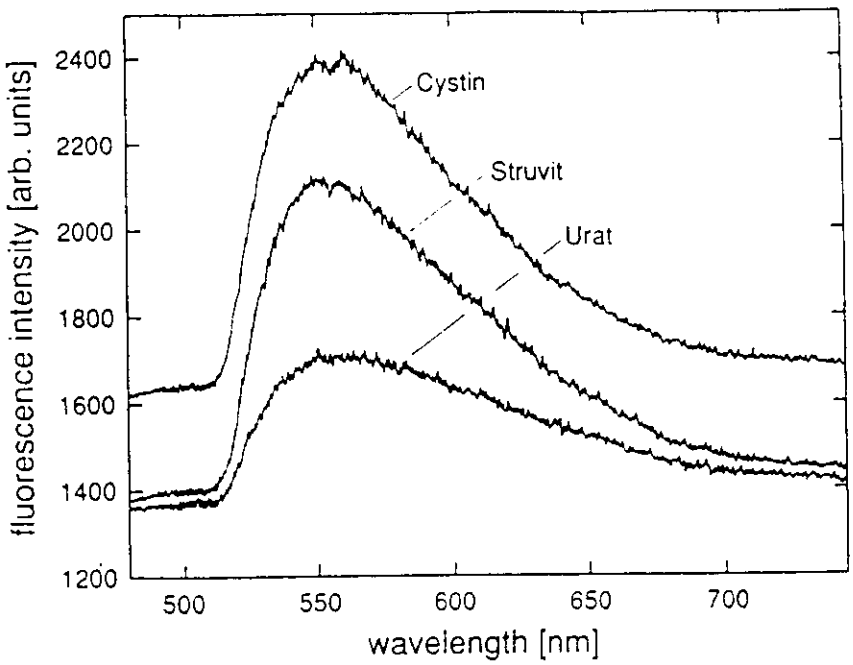

Fig.15.28. Fluorescence of three different kidney-stone materials excited with a dye laser at λ = 497 nm at low intensities to prevent plasma breakdown [15.131]

First demonstrations of the capability of spectral analysis of kidney stones in vitro are illustrated in Fig.15.28 where the fluorescence spectra of different kidney stones which had been irradiated in a water surrounding outside the body, and which were detected with the arrangement of Fig. 15.26, are shown [15.131].

Further information on laser lithotripsy and spectroscopic control of this technique can be found in [15.132, 133].